SYNTHESIS OF SELF–ASSEMBLED POLYSTYRENE NANOSPHERES/CADMIUM METAL NANOPARTICLES (PSNs/CdMNPs) COMPOSITE THIN FILM FOR ITS APPLICATION AS ADSORBENT AND CATALYST

PRATAMA JUJUR WIBOWA

A thesis submitted in fulfillment of the requirement for the award of the Doctor of Philosophy

Faculty of Science, Technology and Human Development
Universiti Tun Hussein Onn Malaysia

MAY, 2015

ABSTRACT

The research described in this dissertation is a comprehensive account of an attempt, for the first time, correlates the secondary pores structural and physicochemical properties of polystyrene nanospheres/cadmium metal nanoparticles (PSNs/CdMNPs) composite thin film with its adsorption and catalytic properties. The PSNs/CdMNPs composites were fabricated on a hydrophilic silicon wafer through self-assembly process from its aqueous colloidal. The existence of secondary pores and atomic particles of cadmium were clarified by using a field emission scanning electron microscopy (FESEM) and an energy dispersive X–ray (EDX) spectroscopy, respectively. Physical and chemical physical stability of the secondary pores were tested toward continuous laser irradiation of 633 nm wavelength and oxygen/argon reactive ion etching (O_2/Ar RIE), respectively. Thermal catalytic effect of CdMNPs was investigated through thermogravimetry/differential thermal analysis (TG/DTA). Any chemical bond change of the PSNs/CdMNPs composite due to both CdMNPs and adsorbate molecules were confirmed by using an attenuated total reflectance–Fourier transform infrared (ATR–FTIR) spectroscopy. The capability of adsorption and catalysis of the secondary pores were clarified to adsorb and degrade tartazine as a model compound. It was found that the fabricated secondary pores were composed of dumbbell-like nanostructure with >100 nm pores in size had better adsorption capability than other adsorbents. It was demonstrated that the Freundlich constants ratio expressed as K_F/n was 1.715×10^4. This value is much higher than previously reported for coconut shell activated carbon (CSAC), *i.e*. 0.158 and commercial activated carbon (CAC), *i.e*. 0.403. The rate of catalytic degradation of tartrazine on secondary pores was 0.718 μmol min^{-1} and a good agreement with pseudo first–order kinetics. Nanostructures of the secondary pores of PSNs/CdMNPs were not significantly changed under 633 nm continuous laser irradiation for 20 minutes as well as under O_2/Argon RIE (30 sccm argon flow rate, 15 sccm oxygen flow rate, 20 seconds) suggesting a strong structural integrity of the secondary pores. Based on these results, it was concluded that PSNs/CdMNPs composites thin film secondary pores showed the adsorption and catalytic capabilities and is considered a potential adsorbent and catalyst.

ABSTRAK

Penyelidikan yang diterangkan dalam disertasi ini adalah penjelasan percubaan yang komprehensif, untuk pertama kalinya, untuk mengaitkan sifat-sifat struktur dan fisikokimia liang sekunder daripada filem nipis komposit polistirena nanosfera/kadmium logam nanopartikel (PSNs/CdMNPs) dengan penjerapan dan sifat pemangkin. Komposit PSNs/CdMNPs telah difabrikasi pada wafer silikon hidrofilik melalui proses memasang diri daripada koloid berair itu. Kewujudan liang sekunder dan adanya partikel atom kadmium deselidiki masing-masing dengan menggunakan mikroskop imbasan pelepasan elektron (FESEM) dan spektroskopi tenaga serakan sinar–X (EDX). Ketahanan fizikal dan kimia liang sekunder itu diuji masing-masing dengan penyinaran laser berterusan 633 nm dan pemaparan ion reaktif oksigen/argon (O_2/Ar RIE). Sifat pemangkin CdMNPs disiasat melalui termogravimetri/pembezaan analisis terma (TG/DTA). Apa-apa perubahan ikatan kimia daripada komposit PSNs/CdMNPs kerana kewujudan CdMNPs serta kehadiran molekul terjerap disahkan dengan menggunakan spektroskopi mengubah pantulan–inframerah Fourier yang dilemahkan (ATR–FTIR). Keupayaan penjerapan dan pemangkinan daripada liang sekunder komposit PSNs/CdMNPs diuji untuk menjerap dan untuk mendegradasi tartazine sebagai sebatian model. Ditemukan keputusan daripada FESEM yang menunjukkan pembentukan liang sekunder di PSNs/CdMNPs yang terdiri daripada bahan berstruktur nano yang berbentuk seperti halter dengan liang sekunder bersaiz > 100 nm. Struktur liang sekunder ini mempunyai keupayaan penjerapan tartrazin yang lebih tinggi berbanding dengan adsorben lainnya yang terbuat dari pada liang primer. Hal ini terlihat dari nisbah pemalar Freundlich daripada liang sekunder komposit PSNs/CdMNPs yang dinyatakan sebagai K_F/n adalah 1.715×10^4. Nilai ini adalah lebih tinggi daripada yang dilaporkan sebelum ini bagi karbon tempurung kelapa aktif (CSAC), iaitu 0.158 dan karbon aktif komersial (CAC), iaitu 0,403. Ciri degradasi tartrazine kerana kewujudan CdMNPs dalam liang sekunder bersesuaian dengan kinetika derajat pertama semu dengan laju degradasi 0.718 μmol min^{-1}. Nanostruktur liang sekunder PSNs/CdMNPs tidak ketara berubah di bawah penyinaran laser berterusan 633 nm selama 20 minit dan juga O_2/Argon RIE (30 sccm kadar aliran argon, 15 sccm kadar aliran oksigen, 20 saat) menunjukkan integriti struktur yang kuat daripada liang sekunder itu. Berdasarkan keputusan ini, dapat disimpulkan bahawa liang sekunder filem nipis komposit PSNs/CdMNPs menunjukkan penjerapan dan keupayaan pemangkin dan dianggap sebagai adsorben dan pemangkin yang berpotensi.

CONTENTS

LIST OF TABLES

LIST OF FIGURES

LIST OF SYMBOLS

% v/v	Volume–volume percentage, that is equal to the volume of solute in milliliter per its 100 milliliter solution.
% w/v	Weight-volume percentage, that is equal to the mass of solute in gram per its 100 milliliter solution..
% w/w	Weight-weight percentage, that is equal to the mass of solute in gram per its 100 gram solution. This is the same as weight percentage term.
% PSNs	Weight percentage of PSNs particles
κ	Tartrazine adsorption proportional constant
π *(pi)* bonding	Overlapping *p* orbital of bonded atoms
π *(pi)* constant	3.14159
φ_1, φ_2, φ_3, φ_4	Rotation angle (0–360^{o}) of tartrazine molecules on its mass center
θ_1, θ_2, θ_3, θ_4	Standing angle (0–90^{o}) of secondary pore
Δt	Temperature different between two states in ^{o}C
3–p	three PSNs particles
4–nop	four–non–ordered PSNs particles
4–op	four–ordered PSNs particles
5–p	five– PSNs particles
Å	Angstrom, that is equal to 10^{-10} meter
A_1	Triangle–wide peak area of ATR–FTIR spectra in 3125–3000 cm^{-1} wavenumber range

A_2	Triangle–wide peak area of ATR-FTIR spectra in 1400–1300 cm^{-1} wavenumber range
$AMAP_{1\mu LPSNs}$	The amount of metal atomic particle loaded in 1µL volume of its associated PSNs dispersion.
$AP_{PSNs1\mu L}$	The amount of PSNs particles that exist in its 1µL dispersion
AW	Atomic weight of metal atomic particle
b	Langmuir constant that represents adsorption binding site affinity of an adsorbent
Cp	Specific heat capacity at constant pressure
e	electron
E_A	Potential energy of tartrazine
E_B	Potential energy of secondary pore of PSNs/CdMNPs composite thin film
E_{bad}	Energy barrier of adsorption of secondary pore of PSNs/CdMNPs composite thin film
$E_{\mathrm{bad\_Cd}}$	Energy barrier of adsorption due to Cd metal nanoparticles existence
E_C	Potential energy of adsorption process
eV	electron volt
GMPS	Mass in gram unit of metal precursor salt required to prepare its solution stock of 1 M 10 mL
K_{F}	Freundlich constant that represents maximum capacity of adsorption of an adsorbent
M	Molar or mole per liter or mmol per milliliter
n	Freundlich constant that represents intensity of adsorption of an adsorbent
NA	Avogadro number, *i.e.* constant number of 6.023×10^{23} particles per mole of mass itself.
$NaBH_4$	Sodium borohydride

Q_{CdMNPs}	Calor absorbed by CdMNPs
Q^{o}	Langmuir constant that represents maximum capacity of adsorption of an adsorbent
Q_{PSNs}	Calor absorbed by PSNs
$Q_{PSNs/CdMNPs}$	Calor absorbed by PSNs/CdMNPs
Q_r	Calor ratio
r_a	PSNs radii in average
r_b	Metal–covered PSNs radii
r_c	PVP–stabilized metal–covered–PSNs radii
r_m	Metal atomic particle radius in average
$\mathrm{SA_{PSNs}}$	Surface area of PSNs particle
$T\uparrow$	The Real heat
T_a	The amount of adsorbed tartrazine in µmol
T_{gd}	The amount of degradable adsorbed tartrazine in µmol
t_m:	Thickness of covering metal
$\mathrm{T_{MAP}}$	Total amount of metal atomic particles covered fully a surface area of each PSNs particle
t_{MAPS}	Thickness of metal atomic single layer covered the associated PSNs particle
$\mathrm{TMC_{PSNs}}$	Thickness of metal covering a PSNs surface
T_{ngd}	The rest amount of non degradable adsorbed tartrazine in µmol
T_o	Original concentration of Tartrazine solution in % w/v
Tr	The rest amount of non–adsorbed tartrazine in µmol
t_s	Thickness of PVP stabilizer
$\mathrm{V_{MAP}}$	Volume of metal atomic particle
$\mathrm{V_{MAPSL}}$	Volume of metal atomic single layer on a surface of PSNs particle

W	Watt
wt, so, et, nr, up and *lo*	The direction of PVP molecule on stabilizing metal-covered PSNs, where *wt, so, et, nr, up* and *lo* stands for west, south, east, north, upper and lower respectively.
E	Porosity of solid-phase material
η	Tartrazine degradation proportional constant

LIST OF ABBREVIATIONS

ATR-FTIR	Attenuated total reflectance-Fourier transform infrared
a_{DL}	Width area of double layer closed–packed periodical spheres arrays
a_{SL}	Width area of single layer closed–packed periodical spheres arrays
AW	Atomic weight
CAC	Commercial activated carbon
Cap	Capric acid
CCB	Chitosan–coated bentonite
Cd	Cadmium
$Cd(NO_3)_2.4H_2O$	Cadmium nitrate–4–hydrate
CdMNPs	Cadmium metal nanoparticles
cm	centimeter
CMC	Ceramic matrix composite
CSAC	Coconut shell activated carbon
d_{DL}	Interpore distance in double layer closed–packed periodical spheres arrays
DI	Deionized
DLPSA	Double layer closed–packed periodical spheres arrays
d_{PSNs}	Density of PSNs emulsion or PSNs particles mass per 1 cm^3 its volume

d_{SL}	Interpore distance in single layer closed–packed periodical spheres arrays
DTA	Differential thermal analysis
EDX	Energy dispersive X–ray
FESEM	Field emission scanning electron microscope
GAC	Granular activated carbon
GMPS	Mass in gram of metal precursor salt
ICP	Inductive couple plasma
IUPAC	International union of pure and applied chemistry
J	joule
kJ	kilo joule
L	liter
MAC	Maximum adsorption capacity
mg	milligrams
min	minutes
mL	milliliter, that is equal to cm^3
mM	millimolar or mmole per liter
MMC	Metal matrix composite
mmol	millimole
µ	mikron
µmol	mikromole
MNPs	Metal nanoparticles
MolMAP	Mole amount of metal atomic particles required to prepare its solution stock to fully cover 1.5810×10^{14} PSNs particles
MPM	Metal precursor mass in gram for the preparation of 1M 10 mL solution stock

mtorr	Mili torr, that is equal to 1 atmosphere pressure.
MW_{MPS}	Molecular weight of the associated metal precursor salt
MW_{PSNs}	Weight average molecular weight of PSNs
nm	nanometer, that is equal to 10^{-9} meter
NM	non-metal
nmol	nanomole, that is equal to 10^{-9} mole
PMC	Polymer matrix composite
PS	Polystyrene
PSNs	Polystyrene nanospheres
RF	Radio frequency
RIE	Reactive ion etching
SA_{PSNs}	Surface area of a PSNs particle body
sccm	second per cubic centimeter
SEM	Scanning electron microscope
SLA	Scanned laser annealing
SLPSA	Single layer closed–packed periodical spheres arrays
TEM	Tunneling electron microscope
TFL	Thin film layer
T_g	Glass transition temperature
TG	Thermo gravimeter/thermo gravimetri
UV-Vis	Ultraviolet-visible
VE_{PSNs}	Volume of PSNs suspension which is introduced for preparing PSNs–metal colloids
V_{MAP}	Volume of metal atomic particle
V_{MAPSL}	Volume of metal atomic single layer on a surface of PSNs

VMP	Volume of a metal atomic particle
VMT_{PSNs}	Volume of metal thickness covered a PSNs surface
VS_{PSNs}	Volume of PSNs suspension which employed to prepare an aqueous colloidal PSNs–metal nanoparticles

LIST OF APPENDICES

CHAPTER 1

INTRODUCTION

1.1 Background

Recently, composite materials have attracted a great deal of attention due to its advantageous properties for various applications in the development of products in various aspects of human life. It is because the properties of composites are closely related to their constituent materials which are significantly different physical or chemical properties, and the materials work together to provide the composite unique properties [1–4]. Among of the composites materials, specifically, a porous polymeric matrix composite (PMC) of metal nanoparticles (MNPs) has shown very useful adsorptive and catalytic properties. They have a variety of application in the fields of sensors, controlled-drug-released agents and column-packing material [5–8], refining and chemical industry, fuel cells and photovoltaic cells [9], air purification, sewage disposal, environmental pollution control and medicine filtering [10–12] and so on. The physical and chemical properties of the composites are significantly enhanced when one of its constituents is within 1–100 nm in size, namely nanocomposite materials [2,13–14]. In this situation, the nanocomposites have special physico–chemical properties due to the quantum size effect and high specific surface area to volume ratio which are different from their atomic or bulk counterparts [15–17].

Nanoparticles of the transition metal oxides (TiO_2, CuO, ZnO)[1,18,19] and the transition metals (Ag, Au, Co, Pt, Fe, Zn, Cd)[7,8,20–22] are widely used as the constituents for the polymer/MNPs composite-based porous materials manufacturing for diverse applications. For instance, Jundale and his co-workers [1] have synthesized polyaniline/CuO nanocomposite for an optical and electrical transport material. Sandoval *et al*. [18] have synthesized a novel extruded polystyrene/TiO_2 nanocomposite material to degrade dye. Mu and his research team [22] have synthesized polyimide/ZnO nanocomposite for photoluminescence material. Another group of researchers [23] has synthesized polystyrene microfibers/CdS nanocomposite for electrical and optical material. Several previous works focused on composite/nanocomposite materials are listed in Appendix A.

Almost all of the polymer matrixes mentioned above were porous solid-phase structure [1,19,22,23] of intraparticle pores type [24–26]. This is a big problem for the development of porous material engineering because the intraparticle pores are very difficult to be generated. The intraparticle pores generation always occur through polymerization process that requires many kinds of chemicals and this results in the difficulties to manufacture intraparticle pores-based porous materials with controllable size and shape [13,27,28]. In this context, it has been accepted that size, shape, and distribution of the pores are three very important factors in generating characters of the porous nanocomposite materials [15,18].

To date, many studies of the porous materials are commonly employing intraparticles pores-based porous materials [13,29] rather than interparticle pore–based ones. This is because the first type of material is more dominant in surface area compared to the associated solid materials formed, as they are smaller in size, that provides higher total surface area to volume ratio than the second type of material [24].

However, uncontrollable size, shape and uniformity of the intraparticle pores become a very serious problem for the porous nanocomposites' fabrication and development. It is because intraparticle pores generation always occur through polymerization process which requires many kinds of chemicals [13,27,28]. Therefore interparticle pores are considered more controllable in size and shape to fabricate porous composite-based materials. In this research, aqueous monodispersion of polystyrene nanosphere (PSNs) of 200 nm size in average is used as polymeric matrix for the intended porous composite thin film material. Study of the relationships of the size and shape with their adsorption and catalytic properties will be focused on the interparticles pores–based porous composite materials. Furthermore, the terms of primary pores and secondary pores will be used in this thesis instead of intraparticle pores and interparticle pores respectively.

Adsorption and catalytic properties of the porous material are easier to be studied when it is in a solid phase. In particularly thin film solid–phase materials, they are commonly prepared as a colloidal system in the most suitable liquid medium to obtain nanoscale–size, shape and particles uniformity [2,30–32]. In the colloidal system, there are at least two kinds of components which are a dispersing medium as a continuous phase (including colloidal stabilizer) and dispersible particles of about 1 nm–1 µm in size [13,33–35].

Deposition of the colloidal system mentioned above on a convenient solid support material (noted as substrate) leads to self-assembly process [2,36–39]. However, cadmium metal nanoparticles (CdMNPs) have never been applied as a counterpart component in the fabrication of porous polymeric matrix composite material. It is commonly used either as CdS or CdSe for light-emitting device and solar cells that is incorporated into the polymer [40,41]. Therefore, we use CdMNPs metal nanoparticles instead of CdS and CdSe as a counterpart component to fabricate PSNs/CdMNPs composite thin film material with secondary pores generated among the PSNs/CdMNPs composite particles. This is because the study focused on the relationship between the size and shape of the secondary pores and its adsorption and catalytic properties rather than the electronic and electrical properties.

On the other hand, tartrazine (trisodium–5–hydroxy–1–(4–sulfonatophenyl)–4–(4–sulfonato–phenylazo)–H–pyrazol–3–carnoxylate)[42] is one of the synthetic dyes widely used in food; textile and paper coloring processing which has been reported could cause health problems at the level of bronchia and skin [43,44], allergies, asthma, migraine, blurred vision, thyroid cancer, mutagenic and lupus [42,45,46]. Tartrazine can endanger human life if it cannot be managed properly during the production and disposal process. At present, the most common treatment method for removal of tartrazine in waste water stream is adsorption [45–47] and oxidation catalytic degradation using metal oxide (TiO_2) or hydrogen peroxide (H_2O_2) [43–44,48]. By these considerations, tartrazine was used to investigate the adsorption and catalytic properties of the fabricated secondary pores of PSNs/CdMNPs composite thin film material.

1.2 Problem statement

The pore structure of a porous nanocomposite material is revealed from both intraparticle voids (primary pores) and interparticle voids (secondary pores) [24–26]. The shape and size of primary pores as well as pore uniformity are very difficult to be controlled. It is because they are generated from the polymerization reactions which require various kinds of chemicals (initiator, terminator, catalyst and appropriate medium) simultaneously employed [1,6,18,22,49–51]. On the other hand, the chemical as well as physical properties, particularly adsorption and catalytic properties of porous nanocomposite material are strictly determined by size, shape, and uniformity of not only the particles themselves but also the generated pores [2,5,52,53]. Therefore, qualitative classification of primary pores based on the size and shape has been performed [24–26]. They become micropores (the width is smaller than 2 nm), mesopores (the width is between 2 and 50 nm), and macropres (the width is larger than 50 nm), or they are classified as cylindrical shape, ink-bottle shape, and funnel shape. However, secondary pores particularly in terms of the size and shape in correlation to the adsorption and catalytic properties of the associated materials have not been intensively studied yet as indicated by the limited number of papers published about this phenomenon [5,13,24,53]. As long as the time, interparticles voids or secondary pores of spherical shape materials were just utilized for the fabrication of nanostructure materials that commonly applied in lithography field [54,55].

In nanomaterial science and engineering point of view, secondary pores can be utilized as a useful adsorbent since they have loading capacity for adsorptive materials are much bigger than that of primary pores. In addition, the secondary pores can also be used to embed or to incorporate any catalytic material for generating catalytic properties so that the associated incorporated material can be used as catalyst. Therefore, the study of secondary pores of polystyrene nanospheres-based materials in relation to adsorption and catalysis is performed in this research.

For the study, the problems are as follows:

i. How can secondary pores of polystyrene nanospheres-based materials be synthesized and fabricated?
ii. How is the secondary pores surface morphology of the fabricated materials and its physical and chemical stability?
iii. How can the adsorption and catalytic properties of secondary pores of the fabricated polystyrene nanospheres-based materials be investigated?

Secondary pores are also a very important factor which significantly influences the quality of any fabricated porous material [5,24–26,53]. Thus, the novelty and contributions of the study is about secondary pores: synthesis, fabrication, characterization, properties, and possibility of application as adsorbent and catalyst in the removal of tartrazine in correlation to their size, shape and distribution/uniformity.

1.3 Hypothesis

With regards to the definition of interparticle voids (secondary pores) [24–26] and a few references as stated in the previous section [1,6,18,49–51], the hypotheses are as follows:

i. PSNs-based secondary pores would be fabricated directly from aqueous colloidal PSNs particles without polymerization reactions by gently dropping the colloidal solution onto a hydrophilic silicon wafer surface, and the size and shape of the secondary pores could be enlarged significantly by cadmium metal nanoparticles (CdMNPs) that aggregate deposit between every two PSNs particles.
ii. Physical and chemical stability of the fabricated secondary pores of PSNs/CdMNPs nanocomposite thin film can be increased by CdMNPs.
iii. The capability of adsorption and catalysis properties of the fabricated secondary pores of PSNs/CdMNPs nanocomposite thin film can be investigated by using tartrazine as a water-soluble organic pollutant model.

1.4 Aim

To fabricate polystyrene nanospheres/Cd metal nanoparticles (PSNs/CdMNPs) composite thin film material, explore its physical and chemical properties and apply it for the adsorption of water-soluble colored organic molecules, tartrazine and study of typical catalytic performance of the material.

1.5 Objectives

The objectives of this study are as follows:

i. To fabricate secondary pores of PSNs/CdMNPs composite thin film material and investigate their specific surface morphology to determine their size and shape.
ii. To investigate the secondary pores surface morphology and stability of the fabricated PSNs/CdMNPs composite thin film material.
iii. To investigate the adsorption and catalytic properties of secondary pores of the fabricated PSNs/CdMNPs composite thin film material for removal of tartrazine.

1.6 Scope

In order to achieve the first objective, synthesis of PSNs/CdMNPs composite thin film material via aqueous colloidal system was carried out. It is because the size, shape, and uniformity of PSNs/CdMNPs particles would be generated in a colloidal system [56]. In this colloidal system, Cd metal precursor is reduced to become Cd metal nanoparticles using either chemical reagent ($NaBH_4$) or physical treatment (high frequency ultrasound of 40 kHz for 45 minutes) [50,57,58]. Subsequently, the desired secondary pores of PSNs/CdMNPs composite thin film material were fabricated on a hydrophilic silicon wafer of 1 cm × 1 cm size using gentle dropping method. FESEM was used to explore the surface morphology of the fabricated secondary pores. This surface morphology provides a lot of information about the size, shape and distribution of the secondary pores.

For the second objective, surface morphology of the fabricated secondary pores was explored using FESEM (JEOL JSM–7600 SM17600053, Japan). The success of CdMNPs incorporation onto PSNs particles was confirmed using Energy Dispersive X–ray (EDX) spectrometer (JEOL JSM–7600 SM17600053, Japan). In addition, physical stability of secondary pores of the fabricated PSNs/CdMNPs composite thin film were investigated by continuous laser irradiation of 633 nm wavelength whereas chemical stability of the secondary pores were investigated by oxygen/argon reactive ion exchange (O_2/Ar RIE).

As for the third objective; the optimum size, shape and distribution of the fabricated secondary pores of PSNs/CdMNPs composite thin film materials were used to adsorb tartrazine molecules through incubation method in batch system for a series of time: 5, 10, 15, 20 and 25 minutes under visible light lamps of the laboratory at ambient temperature and pressure. The adsorbed tartrazine in the secondary pores was confirmed by using ATR-FTIR spectrometer (LR 64912C, N3896, Perkin Elmer, U.S.A) equipped with a universal ATR sample holder and spectrum express FTIR software V1.3.2 Perkin Elmer LX100877–1. The adsorption characteristics of the pores were evaluated using both Langmuir and Freundlich isotherm adsorption. The catalytic characters were evaluated based on the curve trend correlated between the amount of tartrazine and adsorption time.

CHAPTER 2

LITERATURE REVIEW

2.1 Introduction

In this chapter, a research study on the synthesis of self-assembled polystyrene nanospheres/cadmium metal nanoparticles (PSNs/CdMNPs) composite thin film for its application as an adsorbent and catalyst in the removal of tartrazine will be thoroughly reviewed.

2.2 Pores Classification

Based on reference [24–26], pore structure of solid materials can be classified into two main types, intraparticle voids (primary pores) and interparticle voids (secondary pores). In particular intraparticle voids, they can be distinguished further based on their size, shape, and interconnection to the surface of the associated particle.

Furthermore, based on the size of the pores, a pore is classified into three types [5,24–26,59]:

i. Micropores that have widths smaller than 2 nm,
ii. Mesopores that have widths between 2 and 50 nm, and
iii. Macropores that have widths larger than 50 nm.

In addition, another size of 1–100 nm can be classified as nanopores since the size range is commonly used as a parameter of nano-scale-size material [2,14,60–62]. Currently, gigaporous material with pore size of 300-500 nm is also known [63]. Based on the shape of the pores, a pore can be further classified into three types [24]:

i. Cylindrical shaped pores,
ii. Ink–bottle shaped pores, and
iii. Funnel shaped pores.

Based on the pore interconnection to the surface, a pore can be classified into two types [24]:

i. Closed pores, and
ii. Opened pores.

Closed pores are defined as pores which are totally isolated from their neighbours, they have no access to the surface of the particle body. On the other hand, opened pores are defined as pores which have continual channel of communication with the external surface of the particle body, it may open only at the end (noted as blind pore or dead-end pore), or may open at two ends (noted as through pore) [24]. In general, schematic illustration of the primary pore structure and configuration model is depicted in Figure 2.1. In special cases, schematic illustration of the primary pore structure and configuration model generated in PSNs particle body was proposed by Wibawa *et al.* (2011)[58] as depicted in Figure 2.2.

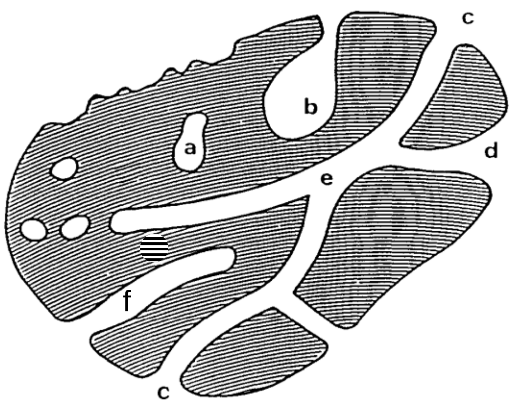

Figure 2.1: Schematic illustration of primary pores classification based on the interconnection to the particle surface, and shape. (a) closed pores; (b, c, d, e) opened pores; (c, e, f) cylindrical shaped pores; (b) ink–bottle shaped pores; (d) funnel shaped pores [24]

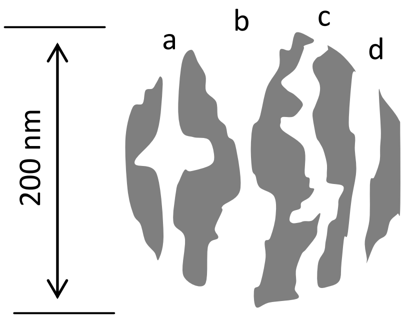

Figure 2.2: Schematic illustration of primary pores models revealed in PSNs particle body of 200 nm size. (a) India traditional trumpet–like pore; (b) face–to–face junction bottle neck–like pore; (c) randomly irregular form pore, and (d) straightforward pipe–like pore

Accordingly, interparticle pore (secondary pore) generated among the PSNs particle bodies can be illustrated as shown in Figure 2.3.

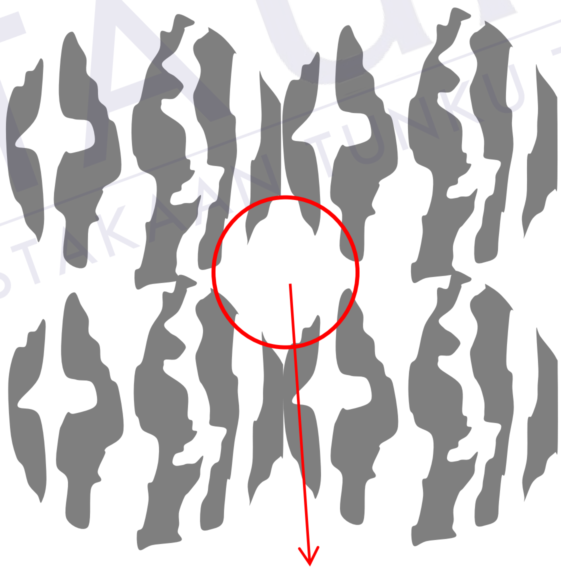

Figure 2.3: Schematic illustration of secondary pores models revealed among four PSNs particle bodies of 200 nm size

The pores and particle size, shape and distribution are the most important parameters for the properties of solid–phase materials in nano–scale–size from 1 nm up to 1µm size range [24–26,64]. It is because within the size, solid-phase materials are dominated by surface properties, including surface area and electrical charge rather than chemical composition of the materials [60]. Interfacial properties are more important for the smaller sizes as the consequence of the mass (atoms) would be at the surface of the particles compared to the bigger sizes [65].

Furthermore, the pore structure of solid-phase materials becomes a main parameter for the porosity (ε) of the associated materials. Porosity is defined as ratio of the total pore volume *Vp* including opened pores and closed pores to the apparent volume *V* of the particle or powder (excluding interparticles voids) [24–26,62]. It is clear that each typical pore provides specific roles that are different from each other in their interactions with other things such as fluids, lights, sounds, and so on. For example, closed pore (Figure 2.1a) is intensively facile for many processes of sound, heat, and light absorptions so that they are beneficial for the manufacturing of vibration dumping material and heat, light even electrical insulators [24–26,62]. Open pores with dead-end are noted as blind open pores (Figure 2.1b and f) which facilitate many processes of adsorptions and catalysis effectively [24–26,62]. In addition, open pores without dead-end are noted as through pores (Figure 2.1c) which facilitate many processes of mass transportation so that they are beneficial in filtration and any material exchange processes [24,62,63].

Accordingly, it can be concluded that pore size and shape as well as their typical distribution are very critical factors in the design and manufacturing process for porous solid nanomaterials for specific applications.

2.3 Primary pores and secondary pore of PSNs/CdMNPs composite thin film

The generation of primary pores and secondary pores of PSNs-based porous materials is also a very critical factor for the development of porous material techniques. In this section, the generation of the typical pores is reviewed in detail.

2.3.1 Primary pores of PSNs/CdMNPs composite thin film

Based on the references [24–26], primary pores (intraparticle voids) of PSNs/CdMNPs composite thin film can be generated by random scaffold of the polystyrene structure network. It has been widely known that polystyrene molecule can exist in three conformation structures due to the rotation of its skeleton carbon-carbon single bonds to synchronize the most stable structure with minimum energy [66–68]. The three conformation structures of polystyrene that are well known are *isotactic*, *syndiotactic* and *atactic* as depicted in Figure 2.4 [68]. The *isotactic* and *syndiotactic* structures usually refer to either crystalline or fibber material whereas *atactic* is usually amorphous [67].

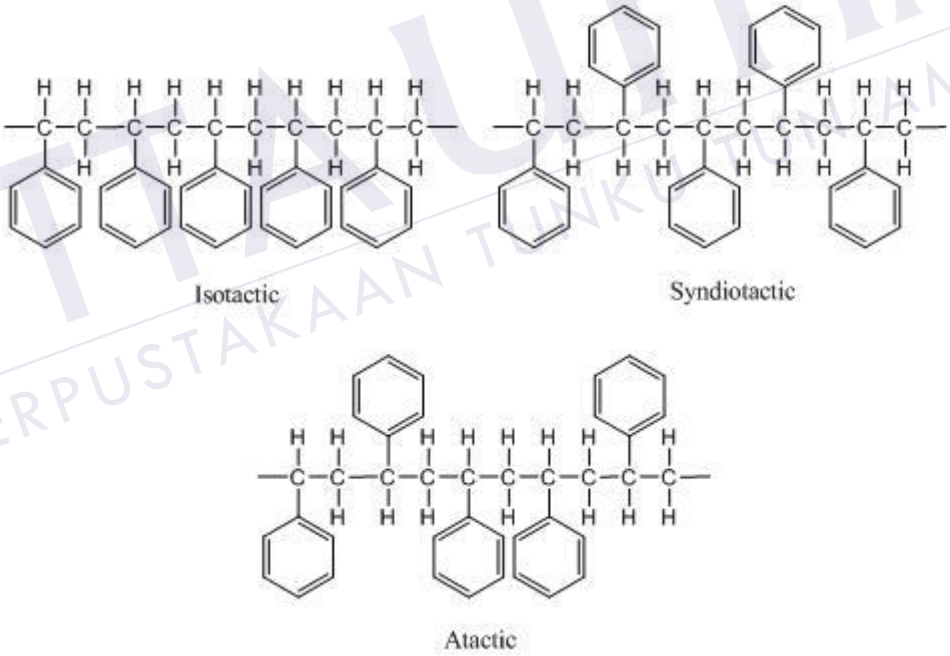

Figure 2.4: Three conformational structures of polystyrene skeleton chain

In the case of *syndiotactic* crystalline structure, it can be α, β, γ and δ crystalline forms depending on the process for getting the crystals [66,69,70]. The most important feature of this phenomenon is its molecular conformational structure. In this context, α and β crystalline forms contain trans-planar zigzag (T_4) conformation that can be obtained by cooling the melted glass or by heating the glass [69]. Whereas γ and δ crystalline forms contain s(2/1)2 helical chains generated by

TTGG conformational sequences that can be obtained by dissolving the polymer into organic solvent (δ form) and subsequently purging away the solvent from the polymer by heating (γ form) [66,70]. Illustration of the molecular chain conformation of the crystalline phases of *syndiotactic* polystyrene is provided by reference [69], Figure 2.5.

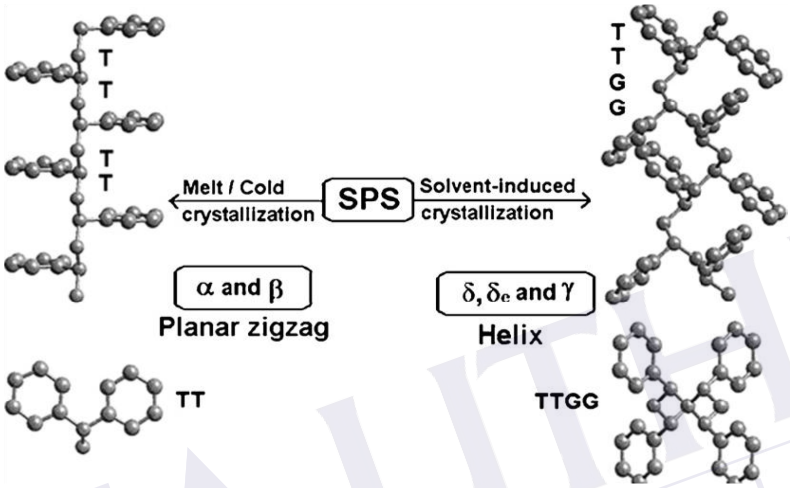

Figure 2.5: Molecular chain conformation of crystalline phases of *syndiotactic* polystyrene [69]

Unfortunately, it still does not provide a clear representation of primary pores generated in PSNs particles particularly in terms of the primary pore shape despite their channels being about 1.5-3.0 nm in size [71]. Researchers [58] have proposed four kinds of valuable models for open primary pores' shape that are possible revealed in the PSNs particles body. The pore models have also been developed based on the capability of multiple random bending and folding of the polystyrene chain frame work. Schematic illustration of the individual primary open pores' models that are possibly revealed in the PSNs particles body is depicted in Figure 2.6.

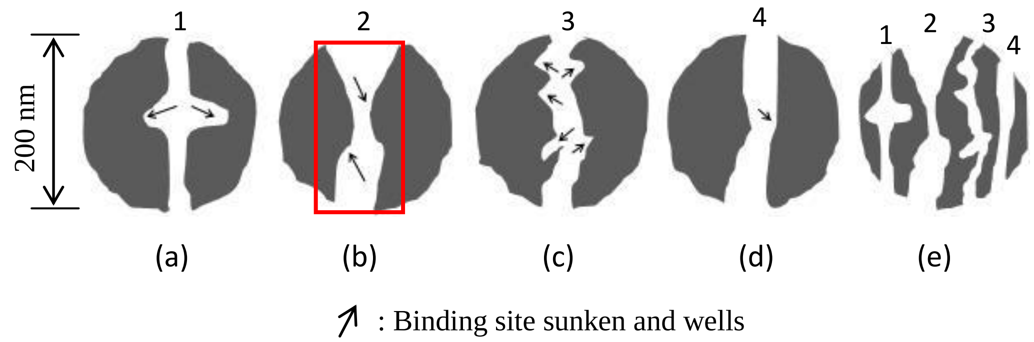

Figure 2.6: Schematic illustration of the individual primary pores models revealed in PSNs particle body of 200 nm size proposed by Wibawa *et al*. (2011)[58]

Figure 2.6a shows an Indian traditional trumpet-like model primary pore, 2.6b face-to-face junction bottle neck–like model primary pore, 2.6c randomly irregular form model, and the last is 2.6d straightforward pipe-like model primary pore. Figure 2.6e represents PSNs particle body with the all primary pore models. The most interesting part of the proposal is the introduction of new terms of nano-sunken and nano-wells that are responsible for effectively binding sites in adsorption and catalytic processes. By using the above models, it is easier to understand that the highest capacity and capability of adsorption will occur on a pore model of irregular form, Figure 2.6c because of the five binding sites which exist therein. On the contrary, the lowest capacity and capability in adsorption will occur on a straightforward pipe-like pore model because it has only one binding site as proposed by Wibawa *et al*. [58].

2.3.2 Secondary pores of PSNs/CdMNPs composite thin film

Based on the reference [24–26], structure of secondary pores (inetrparticles voids) of PSNs/CdMNPs composite thin film would be generated by the ordered and disordered arrangement of the PSNs particles deposited properly on the surface of hydrophilic silicon wafer. In relation to that, each of the researchers [37–39] showed unique secondary pore surface morphology which revealed inter polystyrene particles body of various sizes, 100-500 nm deposited on a solid support material were provided by references [37–39] as seen in Figure 2.7.

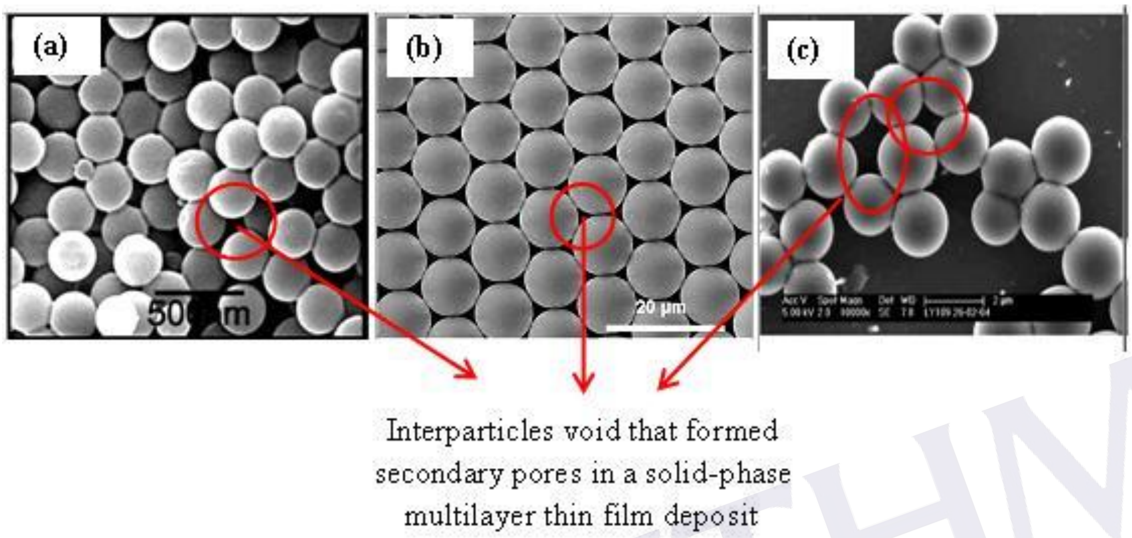

Figure 2.7: FESEM images of (a) secondary pores revealed inter PSNs particles body, multilayer PSNs thin film deposit [37]; (b) ordered single layer PSNs thin film deposit [38]; and (c) disordered single layer PSNs thin film deposit [39].

Figure 2.7a displays various sizes and shapes of secondary pores which revealed inter PSNs particle bodies forming interesting porous nanomaterial structure. The secondary pores structures can be justified clearly by Figure 2.7b and 2.7c where every three close-packed PSNs particles generated triangular shape secondary pores. Figure 2.7c demonstrated the arbitrary configuration of PSNs particles forming a few secondary pores generated by four or five close-packed PSNs particles. If any metal nanoparticles (MNPs) were inserted properly between every two close-packed PSNs particles, the pores will become larger and the capacity of adsorption can be enhanced significantly. In correlation to the definition of nanocomposite material [2,4,14], it means a new useful material namely porous nanocomposite thin film that has capability of adsorption and catalysis can be manufactured properly from PSNs and MNPs particles.

Furthermore porosity of the material can be justified if their volume ratio of pore space to the total volume of the associated material is between 0.20–0.95 [62]. According to the structure and composition of porous material summarized in Table

2.1 [62]; the highest porosity of more than 0.6 commonly belongs to polymer-based materials, so that it is possible to include PSNs particles-based nanocomposite materials.

Table 2.1: Structure and properties/characters relationship of some porous materials based on their main components [62]

NO.	CHARAC-TERISTIC	MATERIALS					
		POLYME-RIC	CAR-BON	GLASS	ALUMI-NA SILICA-TE	OXIDES	METAL
1	Chemical stability	Low-medium	High	High	High	Very high	High
2	Costs	Low	High	High	Low-medium	Medium	Medium
3	Life	Short	Long	Long	Medium-long	Long	Long
4	Permeability	Low-medium	Low-medium	High	Low	Low-medium	High
5	Pore size	Meso up to macro	Micro up to meso	Meso up to macro	Micro up to meso	Micro up to meso	Meso up to macro
6	Porosity	> 0.6	0.3–0.6	0.3–0.6	0.3–0.7	0.3–0.6	0.1–0.7
7	Strength	Medium	Low	Strong	Weak	Weak-medium	Strong
8	Surface area	Low	High	Low	High	Medium	Low
9	Thermal stability	Low	High	Good	Medium-high	Medium-high	High

Table 2.1 shows the relationship of porosity and other properties to the structure and composition of nanocomposite material. Here, for example, organic/inorganic polymeric-based material belongs to meso up to macro pores size, low surface area, porosity > 0.6, low up to medium in permeability, medium in strength, low in thermal stability, low up to medium in chemical stability, low cost and short living time. On the other hand, oxides-based materials possessed meso up to macro pores size, medium surface area, porosity 0.3-0.6, low up to medium in permeability, weak up to medium in strength, medium up to high in thermal stability, very high chemical stability, medium cost and long living time [62].

Specifically, valuable secondary pores-based porous material can be fabricated by means of incorporating CdMNPs to PSNs particles as reported by Wibawa *et al.* (2011)[58]. The incorporated metal will promote hypercrosslinking of the polymer chain and add unique physical properties such as responsiveness to mechanical, optical, thermal and sound barrier, magnetic, electric stimulation [72].

2.4 Synthesis and fabrication of PSNs/CdMNPs composite thin film materials

Secondary pores of PSNs/CdMNPs composite material can be generated only from its aqueous colloid coated on a solid support material. Accordingly, there are two steps to obtain nanostructure secondary pores of the PSNs/CdMNPs composite material. The first step is the synthesis of aqueous colloidal PSNs/CdMNPs composite. The second step is fabrication of secondary pores-based porous PSNs/CdMNPs composite thin film material on a solid support material through deposition method of the colloid. This section describes the two steps.

2.4.1 Synthesis

Referring to previous researches [2,73], PSNs/CdMNPs secondary pores-based porous nanocomposite thin film material can be synthesized by blending Cd metal precursor with numerous PSNs organic polymers. Various polystyrene-based nanocomposite materials had been synthesized using the blending method. Sometimes the blending was performed in solid-phase medium instead of liquid/aqueous medium. For example, silica gel microspheres encapsulated by imidazole functionalized polystyrene (SG–PS–azo–IM) was synthesized and characterized to adsorb transition metals with the highest adsorption capacity for Au(III) from aqueous solution [74]. Polystyrene/carbon nanotubes composites were synthesized by emulsion polymerization with non-covalent and covalent functionalization [75]. Polystyrene/multiwalled carbon nanotubes composites with individual-dispersed nanotubes and strong interfacial adhesion were synthesized in organic mediums of tetrahydrofuran and ethanol [76].

Furthermore, referring to literature [77–79], it can be well understood that the most important things in the synthesis of PSNs/CdMNPs nanocomposites materials is the reduction process of metal precursor used where positive charges ions (cations) become metal (zero valence ions). Many methods have been well known for the reduction of metal precursors which can be distinguished between chemicals methods and physical methods [80]. In this context, chemical methods mean the reduction was performed by employing chemical reducing agent of organic molecule such as *N*,*N*-dimethylformamide (DMF) [77,78,81] and inorganic molecule such as $NaBH_4$ [82] to reduce metal precursor to its metal atom synchronically in a suitable solvent. In contrast, physical reduction methods means that the reduction was performed using physical actions such as high frequency ultrasound of 20 kHz–10 MHz [83,84], microwave irradiation [85–87], gamma (γ) ray radiation [6,88] and so on. In this viewpoint, researchers [80] reported that there were ten various methods of silver nanoparticles preparation by means of reduction process which are well known today.

Physical reduction using high frequency ultrasound would produce metal nanoparticles with lesser chemical contaminants compared to that produced by chemical reducing agents [58,89]. It is also simpler and safer than other physical reductions. In practice, the process of metal precursor reductions could be conducted by means of either *in-situ* in which metal nanoparticles are generated in polymer matrix or *ex-situ* in which metal nanoparticles that were previously synthesized are incorporated in the polymer matrix [2,30,87,90]. In order to make it easy to understand the difference of *in-situ* and *ex-situ* metal reduction process, a simple schematic illustration of both reductions processes is depicted in Figure 2.8.

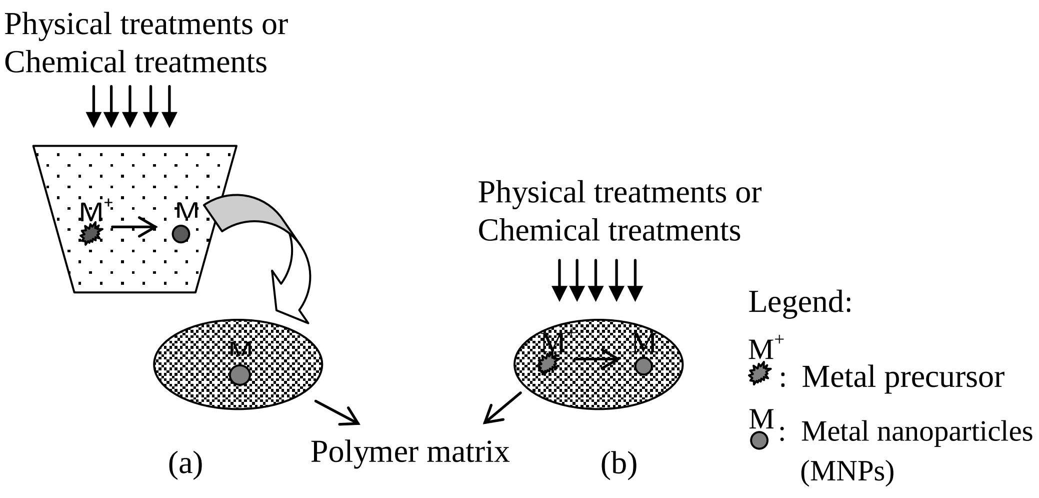

Figure 2.8: Schematic illustration of (a) *ex situ* reduction process of metal precursor M^+ to metal nanoparticles (MNPs) and (b) that of *in situ* one

Figure 2.8a shows metal nanoparticles MNPs were generated on the outside of the supporting matrix material then incorporated into the matrix. In Figure 2.8b metal nanoparticles (MNPs) were generated inside the supporting matrix material.

In addition, the reduction process depends on the purpose for which the nanocomposite is synthesized. Sometimes the *in situ* reduction process is preferred. At other times, the *ex situ* reduction process is prefered. For example, nanocomposite that will be used for adsorbent material will use the *in situ* reduction process whereas the nanocomposite that will be used for catalytic material will use the *ex situ* reduction process. It is because catalytic reactions strictly require a fine condition whereby any poisonous contaminant must be removed from the active side of the catalyst, and this situation will be easier to achieve through *ex situ* method. Detailed comparisons of *in situ* and *ex situ* reduction processes are summarized in Table 2.2.

Table 2.2: Comparison of features of *in situ* and *ex situ* reduction process

NO.	FEATURES	*IN SITU*	*EX SITU*
1	Employing stabilizer [90]	no need	need
2	Employing external reducing agents [90]	no need	need
3	Quality of produced nanoparticles [2]	low	high
4	Synthetic routes for nanoparticles [2]	Just one possible route	Many possible routes can be applied
5	Wide choice of host (supporting matrix) media [2]	Not available	available
6	Control size and shape dependent properties of metal nanoparticles in host matrix [2]	limited	Well controlled

On the other hand, colloidal system with particle size of between 1 nm and 1000 nm (1µm) [89–90] is the best route to produce controllable size, shape and uniformity particles for nanocomposite thin film fabrication [2], including PSNs/CdMNPs composite thin film materials. In this context, water is a common polar solvent for preparing the mixtures of colloidal system particularly for hydrophilic nanoparticles dispersion [33].

Based on reference [34] and adopting the illustration of dispersion structure proposed schematically [35], it can be illustrated schematically the dispersion structure in a continuous phase/dispersion medium of water with modification as depicted in Figure 2.9. Here, water molecules (H_2O) will be capable of forming a liquid matrix through hydrogen bonding networking between them, where many unique cages like cave in nano size are generated in the matrix, of which any dispersed particles reside within the cages.

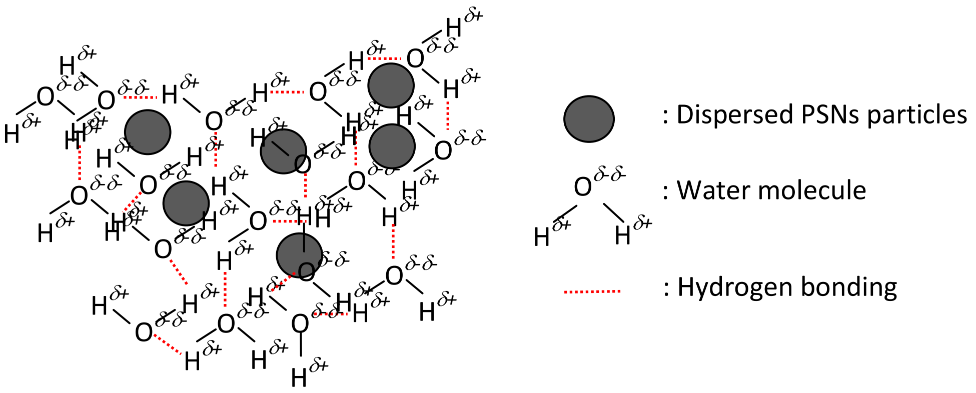

Figure 2.9: Schematic illustration of the structure of dispersion system in water medium

Figure 2.9 shows that particle size ranges from 1–1000 nm for colloidal dispersion system; less than 1 nm for molecular dispersion system that is called solution; and more than 1000 nm for coarse dispersion system that is called suspension.

On the other hand, water molecules are also capable of solvation for any positive and negative electrical charge particles in aqueous system. Solvation itself could be defined as an interaction of a solute with the solvent, which leads to stabilization of the solute species. One may also refer to the solvated state, whereby an ion in a solution is grafted by solvent molecules [91–93]. By this definition, a schematic illustration of the solvated state of positive ion and negative ion could be drawn as depicted in Figure 2.10. It is very clear that the dispersion state and

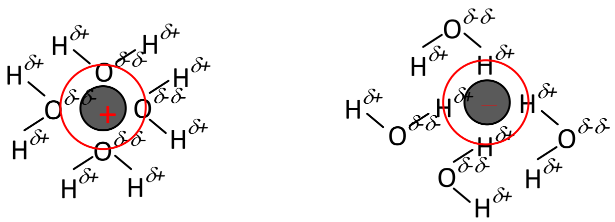

(a) (b)

Figure 2.10: Schematic illustration of (a) solvated state of positive ion and negative ion, and (b) in water

solvated state are very different. Figure 2.10 shows the positive ion surrounded by water molecules through electrostatic force attraction facilitated by water oxygen atom and the associated positive ion, whereas the negative ion was surrounded by water molecules through electrostatic force attraction facilitated by water hydrogen atom and the associated negative ion.

Furthermore, various synthesis methods of CdS/Polystyrene nanocomposite reported by a lot of researchers [39–41,94,95] could be adopted with little bit modification to synthesize PSNs/CdMNPs composite material. The researchers used colloidal stabilizers of either polyvinyl pyrrolidone (PVP) or citric acid [23,41,94,95]. However, in this research did not use colloidal stabilizer because of it can prohibit the capability of adsorption and catalysis of the fabricated secondary pores.

2.4.2 Fabrication

Secondary pores of any solid material including PSNs/CdMNPs composite thin film material could be generated on a solid support material (noted as a substrate) from its suitable liquid colloidal [2,37–39]. In this situation, colloidal particles could initiate in generating both lateral and vertical capillary force between them resulting in the capability of self-assembly which leads to a colloidal thin film forming on a suitable substrate [36]. A schematic illustration of the self-assembly process driven by capillary force which was adopted from literature [36] as shown in Figure 2.11.

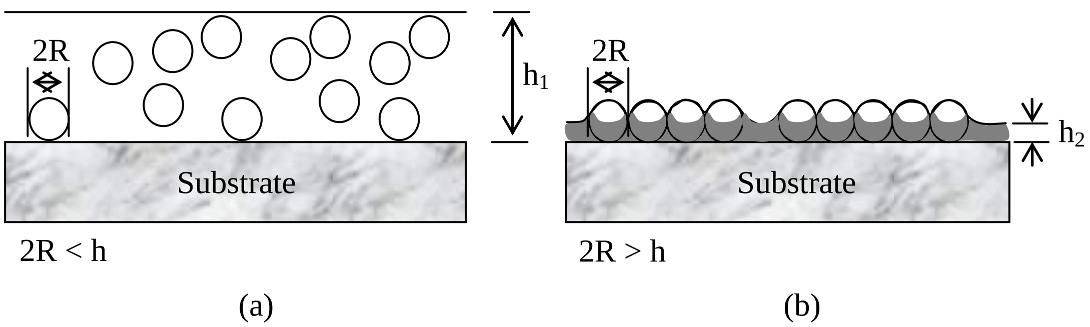

Figure 2.11: Schematic illustration of the self-assembly process drove by capillary force. (a) Lateral capillary forces appear when there is disorderly motion of colloidal particles in a liquid thick layer on a substrate, and (b) ordered state gives rise to aggregation after the top of particles protrude from the liquid layer [36]

Figure 2.11a shows how pressure causes colloidal particles to settle down forming a film while gravity keeps it planar. Figure 2.11b demonstrates a situation that generated lateral capillary forces for a liquid thin film through self–assembly process coinciding with disjoining pressure and three phase contact angle. In this figure, 2R is the diameter (size) of the colloidal particle, h_1: thick liquid layer and h_2: liquid thin layer. Explanation on how the capillary forces appear between colloidal particles had been reported by researchers in reference [36] in detail.

Regarding the specific properties of colloidal system, it is well known that colloidal routes offer numerous advantages for the synthesis of PSNs/CdMNPs nanocomposite thin film material as it allows a good control over size, shape and size distribution of the nanocomposite particles using relatively simple experiment conditions [2,96]. In addition, many researchers proved that a solid nanocomposite thin film material could be manufactured properly on a surface of suitable solid support from its colloidal system by means of drop coating [97–99]; dip coating [31,100–102]; spin coating [103–105]; or spray coating [106–108]. However, the research objectives are about the adsorption phenomenon on secondary pores of the PSNs/CdMNPs nanocomposite thin film materials. Therefore the drop coating technique would be the most convenient technique for manufacturing them since the colloidal PSNs/CdMNPs nanocomposite for generating multilayer secondary pores can be produced in a more controllable quantity [97–99]. In this context, the size of secondary pores in the pattern is proportional to the size of the sphere, and the sphere size of 200 nm is a minimum threshold to get secondary pores of a good shape and size [109].

In addition, the size of secondary pores generated from single layer close packed periodical spheres arrays (SLPSA)(a_{SL}) could be calculated approximately through equation 2.1 while those generated from double layer close packed periodical spheres arrays (DLPSA)(a_{DL}) could be calculated approximately through equation 2.2. Interpores distance in SLPSA (d_{SL}) could be calculated through equation 2.3, whereas interpores distance in DLPSA (d_{DL}) could be calculated through equation 2.4. In this case, it had been shown that triangle–like pores and regular hexagonal pores were revealed in the SLPSA and DLPSA respectively [54,55].

$$a_{SL} = \frac{3}{2}\left[\sqrt{3} - 1 - \frac{1}{\sqrt{3}}\right] D = 0.233 D \quad (2.1)$$

$$a_{DL} = \left[\sqrt{3} - 1 - \frac{1}{\sqrt{3}}\right] D = 0.155 D \quad (2.2)$$

$$d_{SL} = \frac{\sqrt{3}}{D} = 0.577 D \quad (2.3)$$

$$d_{DL} = D \quad (2.4)$$

where *D* is the diameter of polystyrene nanospheres.

2.5 Characterization

A lot of common methods to characterize thin film materials are reviewed in this section. The characterizations of the materials are as the follows.

2.5.1 Thermal properties

Thermal properties of the synthesized PSNs/CdMNPs composites were analyzed using thermogravimetric analysis (TGA) and different thermal analysis (DTA). Under TG analysis, the mass change/degradation of a sample as a function of temperature could be known and well determined. The data output recorded from the TG is a TG curve that correlates sample mass decreasing (Δm) against the temperature progress (T). From the TG curve, the temperature decomposition or thermal stability and glass transition temperature (T_g) of the measured sample [8,17,49,94] will be known. Glass transition temperature itself can be defined as a temperature at which an amorphous solid material becomes soft upon heating or brittle upon cooling. The glass transition temperature will be lower than the melting point of its crystalline form [110]. In relation to this, it is common for CdMNPs to be initially immobilized in the film below the *Tg* of the associated polymer matrices. It is subsequently embedded into the matrices at a temperature above *Tg* since the condition allows the polymer chain to have a high degree of mobility [30].

On the other hand, DTA can be used to measure the difference in temperature change between the sample and reference material both as a function of temperature. The data output recorded from the DTA is a DTA curve that correlates the temperature difference (ΔT) against the temperature progress. Thus, from this DTA curve the typical heat energy accompanied the chemical change of the sample: either exothermic (heat released) or endothermic (heat absorbed) will be known [17,22,110].

Accordingly, it could be concluded that by comparing the data of TG as well as DTA between PSNs/CdMNPs nanocomposite and pristine PSNs it could be known that CdMNPs have been successfully incorporated into PSNs particles. In this context, the quantity of calor (heat energy) required to decompose each material aforementioned is necessary to be determined. For that, the relationship between quantity of calor and temperature that is commonly used to explain the phenomena is expressed in equation 2.5 [111], and this equation can be applied to calculate the calor involved in the mass decomposition process.

$$Q = mCp\Delta t \tag{2.5}$$

where *Q* is heat energy (commonly notes as calor) absorbed, *m* is mass of the degraded material, *Cp* is specific heat capacity of the material and Δ*t* is the temperature difference of the decomposition at the start and final decomposition process that is noted as t_1 and t_2 respectively. In this case, calor quantity expressed in equation 2.5 can be approximately determined based on the TG curves. Based on the TG curves we can determine mass loss of the PSNs/CdMNPs composite as well as that of pristine PSNs at every temperature of the decomposition process where the calculation of calor quantity absorbed by the materials can be obtained.

The most important way to find out the thermal characters of aqueous colloidal PSNs/CdMNPs composite is to investigate its homogenity. Therefore, equation 2.5 needs to be developed to become a more applicable equation. Thus, a valuable equation namely calor ratio (Q_r) that is defined as in equation 2.6 where $Q_{\text{PSNs/CdMNPs}}$, Q_{PSNs}, $\text{Q}_{\text{CdMNPSs}}$ and $\text{m}_{\text{CdMNPSs}}$ are expressesd in equations 2.7, 2.8, 2.9 and 2.10 respectively can be introduced.

REFERENCES

1. Jundale, D. M; Navale, S. T; Khuspe, G. D; Dalavi, D. S; Patil, P. S; and Patil, V.B. (2013). Polyaniline–CuO Hybrid Nanocomposites: Synthesis, Structural, Morphological, Optical and Electrical Transport Studies. *Journal of Material Science:Mater Electron*, 24, pp.3526–3535. DOI: 10.1007/s10854-013-1280-5.
2. Ingrosso, C; Panniello, A. M; Comparelli, R; Curri, M. L. and Striccoli, M.(2010). Colloidal Inorganic Nanocrystal Based Nanocomposites: Functional Materials for Micro and Nanofabrication, *Materials*, 3, pp. 316-1352. DOI:10.3390/ma3021316.
3. Yin, P; Xu, Q; Qu, R; Zhao, G; and Sun, Y. (2010). Adsorption of Transition Metal Ions from Aqueous Solutions onto a Novel Silica Gel Matrix Inorganic–Organic Composite Material. *Journal of Hazardous Materials*, 173, pp. 710–716. DOI:10.1016/j.jhazmat.2009.08.143.
4. Smith,W.F. and Hashemi J. (2006). *Foundations of Materials Science and Engineering*, 4th.Ed. McGraw Hill International Edition, Singapore, pp. 8-15.
5. Vernimmen, J; Meynen, V. and Cool, P. (2011). Synthesis and Catalytic Application of Combined Zeolite/Mesoporous Materials, *Beilstein Journal of Nanotechnology*, 2, pp. 785-801. DOI: 10.3762/bjnano.2.87.
6. Yang, L; Ge, X; Wang, M; Song, L. and He, Xi. (2008a). Preparation of Polystyrene-Encapsulated Silver Hollow Spheres via Self-Assembly of Latex Particles at the Emulsion Droplet Interface, *Materials Letters*, 62, pp. 429-431. DOI: 10.1016/j.matlet.2007.05.057.

7. Wang, C; Huang, C. L; Chen, Y. C; Hwang, G. L; and Tsai, S. J. (2008a). Carbon Nanocapsules-Reinforced Syndiotactic Polystyrene Nanocomposites: Crystallization and Morphological Features, *Polymer*, 49, pp. 5564-5574. DOI: 10.1016/j.polymer.2008.09.057.

8. Wang, L; Wang, F; and Chen, D. (2008b). Fabrication and Characterization of Silver/Polystyrene Nanospheres With More Complete Coverage of Silver Nano-Shell. *Materials Letters,* 62, pp. 2153–2156. DOI:10.1016/j.matlet.2007.11.078.

9. Xie, Z; Liu, Z; Wang,Y; Yang,Q; Xu, L. and Ding,W (2010). An Overview of Recent Development in Composite Catalysts from Porous Materials for Various Reaction and Processes, *International Journal of Molecular Science,* 11, pp.2152-2187. DOI:10.3390/ijms11052152.

10. Ai, L. Zhou, Y. and Jiang J. (2010). Article in Press: Removal of Methylene Blue from Aqueous Solution by Montmorillonite/CoFe2O4 Composite with Magnetic Separation Performance, *Desalination* (2010), DOI:10.1016/j.desal.2010.08.004.

11. El-Latif, A. M. M. El-Kady, M. F. Ibrahim, A. M. and Ossman, M. E. (2010). Alginate/Polyvinyl Alcohol - Kaolin Composite for Removal of Methylene Blue from Aqueous Solution in a Batch Stirred Tank Reactor, *Journal of American Science*, 6(5), pp. 280-292.

12. Zhihua, Z; Jun, S; Xingyuan, N; Yang, L. and Bo, W. Guangming W. Bin, Z. Guoqing, W. Peiqing, W. Qingfeng, W. and Xixian, N. (2008). Benzene adsorption properties of silica aerogel-fiber composite, *2nd IEEE International Nanoelectronic Conference* (INEC 2008), pp. 366-370.

13. Esfandabadi; Maleki, S; Pourmahdian, S; and Khoshkhoo, M. S. (2014). Hollow Spherical Micro/Meso-Porous Silica Structure by Nanospherical Sacrificial Polystyrene Templates. *Journal of Reinforced Plastics and Composites,* 33(5), pp. 401-411. DOI: 10.1177/0731684413503049

14. Paul, D.R and Robeson, L.M.(2008). Polymer Nanotechnology: Nanocomposites, *Polymer,* 49 (15), pp. 3187-3204.DOI: 10.1016/j.polymer.2008.04.017.

15. Chaudhari, S; Shaikh, T; and Pandev, P. (2013). A Review on Polymer TiO_2 Nanocomposites, *International Journal of Engineering Research and Applications*,3(5), pp. pp.1386–1391. ISSN : 2248–9622.
16. Guo, Z; Liang, X; Pereira, T; Scaffaro, R; and Hahn, H. T. (2007). CuO Nanoparticle Filled Vinyl-Ester Resin Nanocomposites: Fabrication, Characterization and Property Analysis. *Composites Science and Technology*, 67, pp. 2036–2044. DOI:10.1016/j.compscitech.2006.11.017.
17. Antolini, F; Pentimalli, M; Luccio, T. D; Terzi, R; Schioppa, M; Re, M; Mirenghi, L. and Tapfer, L. (2005). Structural Characterization of CdS Nanoparticles Grown in Polystyrene Matrix by Thermolytic Synthesis, *Material Letters*, 59, pp. 3181-3187. DOI: 10.1016/j.matlet.2006.08.070.
18. Sandoval, H.G.M; Angarita, B.D.B; Torres, C. S. N.and Pedrozo, P. O. M. (2013). Novel EPS/TiO_2 Nanocomposite Prepared from Recycled Polystyrene, *Material Sciences and Applications*, 4, pp. 179-185. DOI: 10.4236/ msa.2013.43021.
19. Grigalovica, A; Bochkov, I; Meri, R. M; Zicans, J; Grabis, J; Kotsilkova, R; and Borovanska, I. (2012). The Effect of Nanosize ZnO on The Properties of The Selected Polymer Blend Composites. *IOP Conference Series: Materials Science and Engineering*,38, pp. 012053. DOI:10.1088/1757-899X/38/1/012053.
20. Kanahara, M; Shimomura, M. and Yabu, H. (2014). Fabrication of Gold Nanoparticles-Polymer Composite Particles with Raspberry, Core-Shell and Amorphous Morphologies at Room Temperature Via Electrostatic Interactions and Diffusion, *Soft Matter*, 10, pp.275-280. DOI: 10.1039/c3sm52077c.
21. Deniz, A. E; Vural, H. A; Ortaç, B; and Uyar, T. (2011). Gold Nanoparticle/ Polymer Nanofibrous Composites by Laser Ablation and Electrospinning. *Materials Letters*, 65, pp. 2941-2943. DOI:10.1016/j.matlet.2011.06.045.
22. Mu, S; Wu, D; Qi, S; and Wu, Z. (2011). Preparation of Polyimide/Zinc Oxide Nanocomposite Films via an Ion-Exchange Technique and Their Photoluminescence Properties. *Journal of Nanomaterials*, 2011, pp.1-10. DOI: 10.1155/2011/950832.

23. Lu, Xi; Mao, H; Zhang, W. and Wang, C. (2007). Synthesis and Chracterization of CdS Nanoparticles in Polystyrene Microfibers. *Material Letters*, 61, pp. 2288-2291. DOI: 10.1016/j.matlet.2006.08.070.
24. Rouquerol, J; Avnir, D; Fairbridge, C. W; Everett, D.H; Haynes, J. H; Pernicone, N; Ramsay J.D.F; Sing, K.S.W; and Unger, K.K. (1994). Recommendations for The Characterization of Porous Solids (IUPAC recommendations). *Pure & Applied Chemistry*, 66(8), pp: 1739-1758.
25. McCusker, L.B; Liebau, F; and Engelhardt, G. (2001). Nomenclature of Structural and Compositional Characteristics of Ordered Microporous and Mesoporous Materials with Inorganic Hosts (IUPAC recommendations). *Pure & Applied Chemistry*, 73(2), pp: 381–394.
26. Lyklema, J. and van Olphen, H. (1979). Terminology and Symbols in Colloid and Surface Chemistry, part 1.13: Definitions, Terminology and Symbols for Rheological Properties (IUPAC recommendations), *Pure & Applied Chemistry*, 51, pp: 1213–1218.
27. Bidadi, H; Olad, A; Parhizkar, M; Aref, S. M; and Ghafouri, M. (2013). Nonlinear Properties of ZnO-Polymer Composites Prepared by Solution-Casting Method. *Vacuum*, 87, pp. 50-54. DOI: 10.1016/j.vacuum.2012.07.003.
28. Wang, S; Zhang, Z; Liu, H; Zhang, W; Qian, Z; and Wang, B. (2010). One-Step Synthesis of Manganese dioxide/Polystyrene Nanocomposite Foams via High Internal Phase Emulsion and Study of their Catalytic Activity, *Colloid and Polymer Science*, 288, pp. 1031–1039. DOI 10.1007/s00396-010-2236-4.
29. Hua, M.Y; Chen, C. J; Chen, H. C; Rung, Y; Cheng, W; Cheng, C. L; and Liu, Y. C. (2011). Preparation of a Porous Composite Film for the Fabrication of a Hydrogen Peroxide Sensor, *Sensor*, 11, pp. 5873-5885. DOI:10.3390/s110605873.
30. Ali, G; Chen, C; Yoo, S. H; Kum, J. M. and Cho, S. O. (2011). Fabrication of Complete Titania Nanoporous Structures via Electrochemical Anodization of Ti. *Nanoscale Research Letters*, 6(322), pp.1-10. DOI: 10.1186/1556-276X-6-332.
31. Kaneva, N. V. and Dushkin, C. D. (2011). Preparation of Nanocrystalline Thin Films of ZnO by Sol-Gel Dip Coating, *Bulgarian Chemical Communications*, 43(2), pp. 259-263.

32. Naseri, M. G; Saion, E. B; Ahangar, H. A; Shaari, A. H; and Hashim, M. (2010). Simple Synthesis and Characterization of Cobalt Ferrite Nanoparticles by a Thermal Treatment Method, *Journal of Nanomaterials*, 2010, pp. 1-8. DOI:10.1155/2010/907686
33. Sperling, R. A. and Parak, W. J. (2010). Surface Modification, Functionalization and Bioconjugation of Colloidal Inorganic Nanoparticles, *Philosophical Transaction of the Royal Society A,* 368, pp. 1333-1383. DOI: 10.1098/rsta.2009.0273.
34. Nalwa, H.S. (Editor). (2000). *Handbook of Nanostructured Materials and Nanotechnology*, 5, Academic Press, New York, USA, pp. 501-575.
35. Lin, L. (2003). Mechanisms of Pigment Dispersion, *Pigment & Resin Technology,* 32(2), pp. 78 – 88. DOI 10.1108/03699420310464784.
36. Kralchevsky, P. A and Nagayama, K. (1994). Capillary Forces between Colloidal Particles, *Langmuir*, 10, pp. 23–36. DOI: 10.1021/la00013a004.
37. Haldorai, Y. Lyoo, W. S; Noh, S. K. and Shim, J.J. (2010). Ionic Liquid Mediated Synthesis of Silica/Polystyrene Core-Shell Composite Nanospheres by Radical Dispersion Polymerization, *Reactive & Functional Polymers*, 70, pp. 393–399. DOI:10.1016/j.reactfunctpolym.2010.03.009.
38. Mathur, A; Roya, S.S; Hazra, K.S; Misra, D.S. and McLaughlin, J.A. (2010). Growth of Carbon Nanotube Arrays Using Nanosphere Lithography and Their Application in Field Emission Devices, *Diamond & Related Materials*. Articles in Press. DOI:10.1016/j.diamond.2010.02.042.
39. Li, Y; Chun, E; Liu, Y; Pickett, N; Skabara, P. J; Cummins, S. S; Ryley, S; Sutherland, A. J. and O'Brien, P. (2005). Synthesis and Characterization of CdS Quantum Dots in Polystyrene Microbeads, *Journal of Materials Chemistry*, 15, pp. 1238–1243. DOI: 10.1039/b412317d.
40. Lu, Y; Mei, Y; Schrinner, M; Ballauff, M; Möller; and Breu, J. (2007). In Situ Formation of Ag Nanoparticles in Spherical Polyacrylic Acid Brushes by UV Irradiation. *Journal of Physical Chemistry C*, 111, pp. 7676-7681. DOI: 10.1021/jp070973m.

41. Hulteen, J. C; Treichel, D. A; Smith, M. T; Duval, M. L; Jensen, T. R. and Van Duyne, R. P. (1999). Nanosphere Lithography: Size-Tunable Silver Nanoparticles and Surface Cluster Arrays, *Journal of Physical Chemistry B*, 103, pp. 3854-3863. DOI: 10.1021/jp9904771
42. Wan Ngah, W. S; Ariff, N. F. M. and Hanafiah, M. A. K. M. (2010). Preparation, Characterization, and Environmental Application of Crosslinked Chitosan-Coated Bentonite for Tartrazine Adsorption from Aqueous Solutions, *Water Air Soil Pollutantion*, 206, pp. 225-236. DOI: 10.1007/sl1270-009-0098-5.
43. Morales, G. V; Sham, E. L; Cornejo, R; and Torres, E. M. F. (2012). Kinetics Studies of the Photoctatalytic Degradation of Tartrazine. *Latin American Applied Research*, 42, pp. 45-49.
44. Beach, E. S; Malecky, R. T; Gil, R. R; Horwitz, C. P; and Collins, T. J. (2011). Fe-TAML/Hydrogen peroxide Degradation of Concentrated Solutions of the Commercial Azo Dye Tartrazine. *Catalysis Science and Technology*, 1, pp. 437-443. DOI: 10.1039/c0cy00070a.
45. Wawrzkiewicz, M. and Hubucki, Z. (2009). Removal of Tartrazine from Aqueous Solutions by Strongly Basic Polystyrene Anion Exchange Resins, *Journal of Hazardous Materials*, 164, pp. 502-509. DOI: 10.1016/j.jhazmat.2008.08.021.
46. Mittal, A; Kurup, L; and Mittal, J. (2007). Freundlich and Langmuir Adsorption Isotherms and Kinetics for the Removal of Tartrazine from Aqueous Solutions Using Hen Feathers, *Journal of Hazardous Materials*, 146, pp. 243-248. DOI: 10.1016/j.jhazmat.2006.12.012.
47. Sun, W. L; Qu, Y. Z; Yu, Q; and Ni, J. R. (2008). Adsorption of Organic Pollutants from Cooking and Papermaking Wastewaters by Bottom Ash. *Journal of Hazardous Materials*, 154, pp. 595-601. DOI: 10.1016/j.jhazmat.2007.10.063.
48. Tanaka, K; Padermpole, K. and Hisanaga, T. (2000). Photocatalytic Degradation of Commercial Azo Dyes. *Water Research*, 34(1), pp. 327-333. PII: S0043-1354(99)00093-7.
49. Kamrupi, I.R; Phukon, P; Konwer, B.K; Dolul, S.K.(2011). Synthesis of Silver-Polystyrene Nanocomposite Particles Using Water in Supercritical Carbon Dioxide Medium and Its Antimicrobial Activity, *The Journal of Supercritical Fluids*, 55, pp.1089-1094. DOI: 10.1016/j.supflu.2010.09.027.

50. Zinck, P; Bonet, F; Mortreux, A. and Visseaux, M. (2009). Functionalization of Syndiotactic Polystyrene, *Progress in Polymer Science*, 34, pp. 369-392. DOI: 10.1016/j.progpolymsc.2008.10.003.
51. Chen, J; Yang, G; Zhang, H and Chen, Z. (2006). A review: Non-Cross-Linked Polystyrene Bond Reagents, Catalysis and Synthesis, *Reactive & Functional Polymers,* 66, pp. 1434-1451. DOI: 10.1016/j.reactfunctpolym.2006.04.008.
52. Xiao, G; Gao, P; Wang, L; Chen, Y; Wang, Y. and Zhang, G. (2011). Ultrasonochemical-Assisted Synthesis of CuO Nanorods with High Hydrogen Storage Ability. *Journal of Nanomaterials,* 2011, pp. 1-6. DOI:10.1155/2011/439162.
53. Xu, Y; Zhang, D; Wang, Z.L; Gao, Z, T; Zhang, P.B. and Chen, X, S. (2011). Preparation of Porous Nanocomposite Scaffolds with Honeycomb Monolith Structure by One Phase Solution Freeze-Drying Method, *Chinese Journal of Polymer Science*, 29(2), pp. 215-224. DOI: 10.1007/s10118-010-1015-5.
54. Haynes, C. L. and Van Duyne, R. P. (2001). Nanosphere Lithography: A Versatile Nanofabrication Tool for Studies of Size-Dependent Nanoparticles Optics. *Journal of Physical Chemistry B*, 105, pp. 5599-5611. DOI: 10.1021/jp010657m.
55. Hulteen, J. C. and Van Duynea, R. P. (1995). Nanosphere lithography: A materials general fabrication process for periodic particle array surfaces. *Journal of Vacuum Science & Technology A,* 13(3), pp. 1553-1558. DOI: 10.1116/1.579726.
56. Shukla, N; Svedberg, E. B; Ell, J. and Roy, A. J. (2006). Surfactant Effects on the Shape of Cobalt Nanoparticles, *Materials Letters*, 60, pp. 1950-1955. DOI: 10.1016/j.matlet.2005.12.057.
57. Pavanelli, S. P; Bispo, G. L; Nascentes, C. C. and Augusti, R. (2011). Degradation of Food Dyes by Zero-Valent Metals Exposed to Ultrasonic Irradiation in Water Medium: Optimization and Electrospray Ionization Mass Spectrometry Monitoring, *Journal of the Brazilian Chemical Society*, 22(1), pp.111-119. DOI: 10.1590/S0103-50532011000100015.

58. Wibawa, P.J; Saim, H; Agam, M.A. and Nur, H. (2011), Design, Preparation and Characterization of Polystyrene Nanospheres Based-Porous Structure towards UV-Vis and Infrared Light Absorption, *Physics Procedia, 22*, pp. 524 – 531. DOI:10.1016/jphpro.2011.11.081.
59. Ha, T. J; Im, H. G; Yoon, S. J; Jang, H. W. and Park, H. H. (2011). Pore Structure Control of Ordered Mesoporous Silica Film Using Mixed Surfactants. *Journal of Nanomaterials*, 2011, pp. 1-5. DOI: 10.1155/2011/326472.
60. Lead, J. R. and Wilkinson, K. J. (2007). Environmental Colloids and Particles: Current Knowledge and Future Development, Book Chapter, IUPAC, pp.1-15.
61. Jordan, J; Jacob, K. I; Tannenbaum, R; Sharaf, M. A. and Jasiuk, I. (2005). Experimental Trends in Polymer Nanocomposites- A Review. *Material Science and Engineering A*, 393, pp.1-11. DOI: 10.1016/j.msea.2004.09.044.
62. Lu, G.Q. and Zhao, X.S. (2005). Nanoporous Materials-An Overview, *Nanoporous Materials: Science and Engineering E-book*, Chapter 1, released 2005-00.00, Imperial College Press, pp.1-12.
63. Qu, J. B; Huang, Y. D; Jing, G. L; Liu, J. G; Zhou, W. Q; Zhu, H. and Lu, J. R. (2011). A Novel Matrix Derived from Hydrophilic Gigaporous Polystyrene-Based Mirosphere for High-Speed Immobilized-Metal Affinity Chromatography. *Journal of Chromatography B*, 879, pp. 1043-1048. DOI: 10.1016/j.jchromb.2011.03.015.
64. Baset, S; Akbari, . and Zeynali, H. (2011), Size Measurement of Metal and Semiconductor Nanoparticles via UV-Vis Absorption Spectra, *Digest Journal of Nanomaterial and Biostructures*, 6(2), pp. 709-716.
65. Dowling, A. (2005). *Nanoscience and Nanotechnologies: Opportunities and Uncertainties*. Royal Society/Royal Academy of Engineering, London.
66. Uda, Y., Kaneko, F. and Kawaguchi, T. (2004). Guest Exchange Process in Syndiotatic Polystyrene Thin Films Measured by ATR-FTIR Spectroscopy, *Polymer*, 45, pp.2221-2229. DOI: 10.1016/j.polymer.2004.02.004.
67. Odian, G.(1991). *Principles of Polymerization*, 3rd. Ed., John Wiley & Sons, New York, p.27. published on line by Polymer Science Learning Center, Copyright ©2005 Department of Polymer Science The University of Southern Mississippi, USA. Source URL: http://www.pslc.ws/macrog/crystal.htm. Retrieved September 24, 2012.

68. Billmeyer, JR. F.W. (1984). *Textbook of Polymer Science*, 3rd.Edition, Wiley-Interscience Publication John Wiley & Sons, New York, pp. 262-265.

69. Gowd, E.B., Tashiro, K. and Ramesh, C. (2009). Structural Phase Transition of Syndiotactic Polystyrene, *Progress in Polymer Science*, 34, pp. 280-315. DOI: 10.1016/j.progpolymsci.2008.11.002.

70. Albunia, A. R., Musto, P. and Guerra, G. (2006). FTIR Spectra of Pure Helical Crystalline Phase of Syndiotatic Polystyrene, *Polymer*, 47, pp. 234-242. DOI: 10.1016/j.polymer.2005.10.135.

71. Tsyurupa, M.P; Blinnikova, Z.K; Proskurina, N.A; Pastukov, A.V; Pavlova, L.A. and Davankov, A.V. (2009). Hypercrosslinked Polystyerene: The First Nanoporous Polymeric Material, *Nanotechnologies in Rusia*, 4(9-10), pp. 665-675. DOI: 10.1134/S1995078009090109.

72. Schexnailder, P. and Schmidt, G. (2009). Nanocomposite Polymer Hydrogels, *Colloidal Polymer Science*. 287, pp. 1-11. DOI: 10.1007/s00396-008-1949-0.

73. Shen, J and Chan, Y.C. (2009). Research Advances in Nano-Composite Solders, *Microelectronics Reliability*, 49, pp. 223–234. DOI: 10.1016/j.microrel.2008.10.004.

74. Yin, P; Xu, Q; Qu, R; Zhao, G. and Sun, Y. (2010). Adsorption of Transition Metal Ions from Aqueous Solutions onto a Novel Silica Gel Matrix Inorganic–Organic Composite Material, *Journal of Hazardous Materials*, 173, pp.710–716. DOI: 10.1016/j.jhazmat.2009.08.143.

75. Khan, M. U; Gomes, V. G. and Altarawneh, I. S. (2010). Synthesizing Polystyrene/Carbon Nanotube Composite by Emulsion Polymerization with Non-Covalent and Covalent Functionalization, *Carbon*, Articles in Press. DOI: 10.1016/j.carbon.2010.04.029.

76. Yuan, J. M; Fan, Z. F; Chen, X. Hua; Chen, X. Hong; Wu, Z. J and He, L. P. (2009). Preparation of Polystyrene/Multiwalled Carbon Nanotubes Composites with Individual-Dispersed Nanotubes and Strong Interfacial Adhesion. *Polymer*, 50, pp. 3285-3291.DOI: 10.1016/j.polymer.2009.04.065.

77. Singho, N. D; Johan, M. R; and Che Lah, N. A. (2014). Temperature-Dependent Properties of Silver-Poly(methylmethacrylate) Nanocomposites Synthesized by *in-situ* Technique, *Nanoscale Research Letter*, 942, pp. 1-6. DOI: 10.1186/1556-276X-9-42

78. Sadeghi, B. and Pourahmad, A. (2011). Synthesis of Silver/Poly(diallyldimethyl ammonium chloride) hybride Nanocomposite. *Advanced Powder Technology*, Articles in Press. DOI: 10.1016/j.apt.2010.10.001.
79. Shukla, N; Svedberg, E. B; Ell, J. and Roy, A. J. (2006). Surfactant Effects on the Shapes of Cobalt Nanoparticles, *Materials Letters*, 60, pp. 1950-1955. DOI: 10.1016/j.matlet.2005.12.057.
80. Zhang, W; Qiao, X. and Chen, J. (2007). Synthesis of Silver Nanoparticles-Effect of Concerned Parameters in Water/Oil Microemulsion, *Materials Science and Engineering B*, 142, pp. 1-15. DOI: 10.1016/j.mseb.2007.06.014.
81. Choi, Y. J; Chiu, C. K. and Luo, T.J.M. (2011). Spontaneous Deposition of Gold Nanoparticle Nanocomposite on Polymer Surfaces through Sol-Gel Chemistry. *Nanotechnology*, 22, pp.1-8. DOI: 10.1088/0957-4484/22/4/045601.
82. Wang, L; Yan. L; Zhao, P. and Torimoto, Y. (2008c). Surface Modification of Polystyrene with Atomic Oxygen Radical Anions-Dissolved Solution, *Applied Surface Science*, 254, pp: 4191-4200. DOI: 10.1016/j.apsusc.2008.01.035.
83. Zhang, K.; Park, B.J.; Fang, F.F.; and Choi, H. J. (2009). Sonochemical Preparation of Polymer Nanocomposite, *Molecules*, 14, pp. 2095-2110. DOI: 10.3390/molecules140602095
84. Gedanken, A (2003). Sonochemistry and its Application to Nanochemistry, *Current Science*, 85(12), pp. 1720-1722.
85. Patel, K; Kapoor, S; Dave, D. P. and Mukherejee, T.(2005). Synthesis of Pt, Pd, Pt/Ag and Pd/Ag Nanoparticles by Microwave-Polyol Method, *Journal of Chemical Sciences*, 117(4), pp. 311-316. DOI: 10.1007/BF02708443.
86. Yang, S; Wang, Y; Wang, Q; Zhang, R. and Ding, B. (2007). UV Irradiation Induced Formation of Au Nanoparticles at Room Temperature: The Case of pH Values, *Colloidal and Surface A: Physicochemistry Engineering Aspects*, 301, pp. 174-183. DOI: 10.1016/j.colsurfa.2006.12.051.
87. Balan, L. and Burget, D. (2006). Synthesis pf Metal/Polymer Nanocomposite by UV-Radiation Curing, *European Polymer Journal*, 42, pp. 3180-3189. DOI: 10.1016/j.eurpolymj.2006.08.016.

88. Wu, D; Ge, X; Huang, Y; Zhang, Z. and Ye, Q. (2003). γ-Radiation Synthesis of Silver-Polystyrene and Cadmium Sulfide-Polystyrene Nanocomposite Mirospheres, *Materials Letters*, 57, pp. 3549-3553. DOI: 10.1016/SO167-577X(03)00123-X.
89. Wibawa, P. J., Saim, H., Agam, M.A., Nur, H. (2013). Manufacturing and Morphological Analysis of Composite Material of Polystyrene Nanospheres/ CadmiumMetal Nanoparticles. *Bulletin of Chemical Reaction Engineering & Catalysis*, 7 (3), pp. 224-232. DOI:10.9767/bcrec.7.3.4043.224-232.
90. Si, S; Dinda, E. and Mandai, T. K.(2007). In situ synthesis of Gold and Silver Nanoparticles by using Redox-Active Amphiphiles and Their Phase Transfer to Organic Solvents, *Chemical European Journal*, 13, pp. 9850-9861. DOI: 10.1002/chem..200701014.
91. Lyklema, J; Leeuwen, H. P. van; Vliet Martina and Cazabat, Anne-Marie. (2005), *Fundamentals of Interface and Colloid Science: Particulate Colloids*, 1st Edition, Elsevier Ltd. London, pp. 1-7.
92. Evrett, D. H. (1972), *Definitions, Terminology and Symbols in Colloid and Surface Chemistry*, Adopted by the IUPAC Council at Washington DC USA on July 1971, London, UK.
93. Jenkins, A. (2006). *Updates compiled of IUPAC Compendium of Chemical Terminology*, 2^{nd}. Edition. (the "Gold Book"). Compiled by A. D. McNaught and A. Wilkinson. Blackwell Scientific Publications, Oxford (1997). XML on-line corrected version. Source URL : http://goldbook.iupac.org created by M. Nic, J. Jirat, B. Kosata; ISBN 0-9678550-9-8. DOI:10.1351/goldbook.
94. Yoon, H; Lee, J; Park, D. W; Hong, C. K. and Shim, S. E. (2010). Preparation and Electrorheological Characteristic of CdS/Polystyrene Composite Particles, *Colloidal Polymer Science*, 288, pp. 613-619. DOI: 10.1007/s00396-009-2174-1.
95. Wei, G; Wen, F; Zhang, X; Zhang, W; Jiang, X; Zheng, P. and Shi, L. (2007). A General Method to synthesize of Amphilic Colloidal Nanoparticles of CdS and Noble Metals, *Journal of Colloidal and Interface Science*, 316, pp. 53-58. DOI: 10.1016/j.jcis.2007.07.042.

96. Li, B; Huang, X; Liang, L. and Tan, B.(2010), Synthesis of Uniform Microporous Polymer Nanoparticles and Their Applications for Hydrogen Storage, *Journal of Material Chemistry*, 20, pp. 7444–7450. DOI: 10.1039/c0jm01423k.
97. Saikia, P. J. and Sarmah, P. C. (2011). Investigation of Polyaniline Thin Film and Schottky Junction with Aluminium for Electrical and Optical Characterization, *Materials Sciences and Application*, 2, pp. 1022-1026. DOI: 10.4236/msa.2011.28138
98. Watanabe J; Shen, H; and Akashi, M. (2009). Alternate drop coating for forming dual biointerfaces composed of polyelectrolyte multilayers, *Journal of Material Science*, 20, pp. 759-765. DOI: 10.1007/s10856-008-3615-y.
99. Pang, S. C; Anderson, M. A; and Chapman, T. W. (2000). Novel Electrode Materials for Thin-Film Ultracapacitors: Comparison of Electrochemical Properties of Sol-Gel-Derived and Electrodeposited Manganese Dioxide, *Journal of The Electrochemical Society*, 147(2), pp. 444-450. DOI: 10.1149/1.1393216.
100. Hume, Patrick S; Bowman, Christoper N; and Anseth, Kristi S. (2011). Functionalized PEG Hydrogels through Reactive Dip-Coating for the Formation of Immunoactive Barriers, *Biomaterials*, 32(26), pp. 6204-6212. DOI: 10.1016/j.biomaterials.2011.04.049.
101. Zakaria, N. Z; Amizam, S; and Rusop, M. (2009). SEM Characterization of ZnO Thin Films Deposited by Dip Coating Technique, *AIP Conference Proceeding*, 1136, pp. 786-789. DOI: 10.1063/1.3160257.
102. Brinker, C. J; Frye, G. C; Hurd, A. J; and Ashley, C. S. (1991). Fundamentals of Sol-Gel Dip Coating, *Thin Solid Films*, 201, pp. 97-108. DOI: 10.1016/0040–6090(91)90158-T.
103. Bartlett, A. P; Pichumani, M; Giuliani, M; Viñas, W. G; and Yethiraj, A. (2012). Modified Spin-coating Technique to Achieve Directional Colloidal Crystallization, *Langmuir*, 28, pp. 3067-3070. DOI: 10.1021/la204123s.
104. Suciu, R. C; Roşu, M. C; Silipaş, T. D; Biriş, A, R; Bratu, I; and Indrea, E. (2011). TiO_2 Thin Films Prepared by Spin Coating Technique, *Revue Roumaine de Chimie*, 56(6), pp. 607-612.

105. Hall, D. B; Underhill, P; and Torkelson, J. M. (1998). Spin Coating of Thin and Ultrathin Polymer Films, *Polymer Engineering and Science,* 38(12), pp. 2039-2045. DOI: 10.1002/pen.10373.

106. Nie, W; Coffin, R; Liu, J; MacNeill, Christopher M; Li, Y; Noftle, R. E; and Carroll, D. L. (2012). Exploring Spray-Coating Techniques for Organic Solar Cell Applications, *International Journal of Photoenergy,* 2012, pp. 1-7. DOI: 10.1155/2012/175610

107. Atthi, N; Saejok, K; Supadech, J; Jeamsaksiri, W; and Thongsuk, O. (2010). Improvement of Photoresist Film Coverage on High Topology Surface with Spray Coating Technique, *Journal of the Microscopy Society of Thailand,* 24(1), pp. 42-46.

108. Girotto, C; Rand, B. P; Genoe, J; and Heremans, P. (2009). Exploring Spray Coating as a Deposition Technique of the Fabrication of Solution-Processed Solar Cells, *Solar Energy Materials & Solar Cells,* 93, pp. 454-458. DOI: 10.1016/j.solmat.2008.11.052.

109. Wu, P; Peng, L; Tuo, X; Wang, X; and Yuan, J. (2005). Control of Deposition Channels in Nanosphere Templates for High-Density Nanodot Array Production**,** *Nanotechnology,* 16, pp. 1693–1696. DOI:10.1088/0957-4484/16/9/047.

110. Hatakeyama, T. and Liu, Zhenhai (1998). *Handbook of Thermal Analysis,* John Wiley & Sons, New York. pp. 4, 17-23, 66-73, 304-310.

111. Levine, I. N. (2009). *Physical Chemistry*, 6th. Edition, McGraw-Hill, New York, pp. 46-51.

112. Aufmann, R. N; Barker, V. C and Nation, R.D. (2000). *Precalculus with Limits*, Houghton Mifflin Company, New York, pp. 131-170, 187, 328-330.

113. Cohen, D (1997), Precalculus: *A Problem-Oriented Approach*, 5th. Edition, West Publishing Company, San Fransisco, pp. 57-96, 101-128, 346-348.

114. Bhuvana,T. and Kulkarni, G.U. (2008). Polystyrene as a Zwitter Resist in Electron Beam Lithography Based Electroless Patterning of Gold, *Bulletin of Material Science.,* 31(3), pp. 201-206. DOI: 10.1007/s12034-008-0036-y.

115. Liu, J. (2005). High-Resolution Scanning Electron Microscopy in Yao, N. and Wang, Z. L. *Handbook of Microscopy for Nanotechnology*, 9th.Printed, Kluwer Academic Publishers, Boston, pp. 325-341, 371-387, 399.

116. Silverstein, R.M.; Bassler, G.C. and Morril, T.C. (1981). *Spectrometric Identification of Organic Compounds*, 4th.Edition, John Wiley & Sons, New York.

117. Naim, R; Ismail, A. F; Saidi, H. and Saion, E. (2013). Development of Sulfonated Polysulfonate Membrane as a Material for Proton Exchange Membrane (PEM). URL source: http://www.eprints.utm.my/1937/1/Rosnawati2004-Development of Sulfonatedpolysulfonemembrane. Retrieved May 6, 2013.

118. Luo, H. L; Sheng, J. and Wan, Y. Z. (2008). Preparation and Characterization of TiO_2/Polystyrene Core-Shell Nanospheres via Microwave-Assisted Emulsion Polymerization, *Material Letters*, 62, pp. 37-40. DOI: 10.1016/j,matlet.2007.04.108.

119. Tseng, C. C; Chang, C. P; Ou, J. L; Sung, Y; and Ger, M. D. (2008). The Preparation of Metal-Styrene Oligomer and Metal-SSNa Nanocomposites Through Single Thermal Process, *Colloids and Surface A: Physicochemical and Engineering Aspects*, 330, pp.42-48. DOI:10.1016/j.colsurfa.2008.07.027.

120. Viana, R. B; da Silva, A. B. F. and Pimentel, A. S. (2012). Infrared Spectroscopy of Anionic, Cationic, and Zwitterionic Surfactants, *Advanced in Physical Chemistry*, 2012, pp. 1-14. DOI: 10.1155/2012/903272.

121. Bozkurt, A. (2005). Anhydrous Proton Conductive Polystyrene Sulfonic Acid Membrane, *Turkey Journal of Chemistry*, 29, pp. 117-123.

122. Wu, H.D; Wu, S. C; Wu, I. D. and Chang, F. C. (2001). Novel Determination of The Crystallinity of Syndiotactic Polystyrene Using FTIR Spectrum, *Polymer*, 42, pp. 4719-4725. DOI: 10.1016/S0032-3861(00)00849-1

123. Pfleging, W; Torge, M; Bruns, M; Trouillet, V; Welle, A; and Wilson, S. (2009). Laser- and UV-Assisted Modification of Polystyrene Surfaces for Control of Protein Adsorption and Cell Adhesion. Applied Surface Science, 255, pp. 5453-5457. DOI:10.1016/j.apsusc.2008.08.053.

124. Eliezer, S; Eliaz, N; Grossman, E; Fischer, D; Gouzman, I; Henis, Z; Pecker, S; Horovitz, Y; Fraenkel, M; Maman, S; and Lereah, Y. (2004). Synthesis of Nanoparticles with Femtosecond Laser Pulses. *Physical Review B*, 69, pp. 1441191-1441196. DOI:10.1103/PhysRevB.69.144119.

125. Lu, Y; and Chen, S. C. (2003). Nanopatterning of a Silicon Surface by Near-Field Enhanced Laser Irradiation. *Nanotechnology*, 14, pp. 505-508. PII: S0957-4484(03)56752-6.

126. Zhang, Y.J; Wang, X; Wang, Y; Liu, H. and Yang, J. (2008a). Ordered Nanostructures Fabricated by Nanosphere Lithography. *Journal of Alloys and Compounds*, 452, pp. 473-477. DOI: 10.1016/j.jallcom.2007.11.021.

127. Zhang, Y.J; Li, W. and Chen, K. J. (2008b). Application of Two-Dimensional Polystyrene Arrays in The Fabrication of Ordered Silicon Pillars, *Journal of Alloys and Compounds*, 450, pp. 512-516. DOI: 10.1016/j.jallcom.2006.11.184.

128. Khadom, A. A; Yaro, A. S. and Kadhumi, A. A. H. (2010). Adsorption Mechanism of Benzotriazole for Corrosion Inhibition of Copper-Nickel Alloy in Hydrochloric Acid, *Journal of Chili Chemical Society*, 55(1), pp. 150-152.

129. Tella, A.C and Owalude, S.O. (2007). Some Langmuir and Freundlich Parameters of Adsorption Studies of Chlorphenilamine maleate, *Research Journal of Applied Sciences*, 2(8), pp. 875-878.

130. Awan, M. A; Qazi, I. A. and Khalid, I. (2003). Removal of Heavy Metals through Adsorption Using Sand, *Journal of Environmental Sciences*, 15(3), pp. 413-416.

131. Aksu, Z. (2001). Equilibrium and Kinetic Modelling of Cadmium(II) Biosorption by *C. vulgaris* in a Batch System: Effect of Temperature, *Separation and Purification Technology*, 21, pp. 285–294.

132. Astruc, D. (2007). Trasition-Metal Nanoparticles in Catalysis: From Historical Background to the State-of the-Art. *Nanoparticles and Catalysis*, Astruc, D (Ed.), Wiley-VCH Verlag GmBH & Co, Weinheim, pp.1-33, 255-273.

133. Nur, H. (2006). Fundamental: Heterogeneous Chemocatalysis. *Heterogeneous Chemocatalysis: Catalysis by Chemical Design*, Nur. H (Ed.), Ibnu Sina Institute for Fundamental Science Studies UTM, Johor Bahru, pp. 1-14.

134. Mazaheritehrani, M; Asghari, A; Orimi. R.L; and Pahlavan, S. (2010). Microwave-Assisted Synthesis of Nano-Sized Cadmium Oxide as a New and Highly Efficient Catalyst for Solvent Free Acylation of Amines and Alcohols. *Asian Journal of Chemistry*, 22(4), pp. 2554-2564.

135. Kondawar, S; Mahore, R; Dahegaonkar, A; and Agrawal, S; (2011). Electrical Conductivity of Cadmium Oxide Nanoparticles Embeded Polyaniline Nanocmposites. *Advanced in Applied Science Research*, 2(4), pp. 401-406.
136. Rohovec, J; Touskova, J; Tousek, J; Schauer, F; and Kuritka, I. (2011). New Cadmium Sulfide Nanomaterial for Heterogeneous Organic Photovoltaic Cells. *World Renewable Energy Congress*, 8-13 May, Linköping, Sweden.
137. Sun, Q; Fu, S; Dong, T; Liu, S; and Huang, C. (2012). Aqueous Synthesis and Characterization of TGA-Capped CdSe Quantum Dots at Freezing Temperature. *Molecules*, 17, pp. 8430-8438. DOI: 10.3390/molecules17078430.
138. Li, S; Lin, M. M; Toprak, M. S; Kim, D. K; and Muhammed, M. (2010). Nanocomposites of Polymer and Inorganic Nanoparticles for Optical and Magnetic Applications. *Nano Review*, 1, pp. 5214-5235. DOI: 10.3402/nano.v1i0.5214.
139. Muraviev, D. N., Macanás, J., Ruiz, P. and Muñoz, M. (2008), Synthesis, Stability and Electrocatalytic Activity of Polymer-Stabilized Monometallic Pt and Bimetallic Pt/Cu core–shell nanoparticles. *Physica Status Solidi A*, 205(6), pp. 1460–1464. DOI: 10.1002/pssa.200778132.
140. Novik, A.A. (2010). *Applying of Ultrasound for Production of Nanomaterials*, XXII Session of the Russian Acoustic Society, Session of the Scientific Council of Russian Academy of Science on Acoustic, Moscow. pp. 15-17.
141. Campos, M.D.; Muller, F.A.; Bressiani, A.H.A.; Bressiani, J.C. and Greil, P. (2007). Sonochemical Synthesis of Calcium Phosphate Powders, *Journal of Material Science: Materials in Medicine*, 18, pp. 669-675. DOI: 10.1007/s10856-006-0006-0
142. Naddeoa, V.; Belgiornoa, V. and Napolib, R.M.A. (2007). Behaviour of Natural Organic Matter during Ultrasonic Irradiation, *Desalination*, 8, pp. 40-44. DOI: 10.1016/j.desal.2006.05.042
143. O’Donnell, B. A; Li, E.X.J; Lester, M.I; and Fransisco, J. S. (2008). Spetroscopic Identification and Stability of the Intermediate in the OH + $HONO_2$ Reaction, *Proceeding of the National Academy of Science*, 105(35), pp. 12678-12683. DOI: 10.1073/pnas.0800320105.
144. Gokel, G. W (2004). *Dean’s Handbook of Organic Chemistry*. 2^{nd}. Edition. Mc.Graw-Hill. New York.

145. Lide, D. R. (Editor-in –Chief)(2000). *Handbook of Chemistry and Physics*. 81st. Edition. CRC Press. New York.
146. Kaye, G.W.C and Laby, T.H. (1995). *Table of Physical and Chemical Constants*, 16th. Edition, Logman. Source URL: http://www.rsc.org/periodic-table/element. Retrieved: May 15, 2012.
147. Smith, D. H. (1999). Grignard Reactions in Wet Ether. *Journal of Chemical Education*, 76(10), pp. 1427, Bibcode:1999JChEd..76.1427S, DOI:10.1021/ed076p1427.
148. Solomons, T. W. G. and Fryhle, C.B. (2008). *Organic Chemistry*, 9th. Edition, John Wiley & Sons, Singapore, pp. 30-31.
149. Bruckner, R. (2002). *Advanced Organic Chemistry: Reaction Mechanism*, A Harcourt Science and Technology Academic Press, San Diego, pp. 5-20, 85.
150. Nurmukhametov, R. N; Volkova, L. V; and Kabanov, S. P. (2006). Fluorence and Absorption of Polystyrene Exposed to UV Laser Radiation, *Journal of Applied Spectroscopy*, 73(1), pp: 55- 60. UDC 535.37+541.14.
151. Duan, H; Zhao, J; Zhang, Y; Xie, E; and Han, L. (2009). Preparing Patterned Carbonaceous Nanostructures Directly by Overexposure of PMMA Using Electrob-Beam Lithography. *Nanotechnology*, 20, pp:1- 8. DOI: 10.1088/0957-4484/20/13/13530.
152. Liu, Q. Q; Wang, L; Xiao, A. G; Yu, H. J; and Tan, Q. H. (2008). A Hyper-Cross-Linked Polystyrene with Nano-Pore Structure. *European Polymer Journal*, 44, pp: 2516-2522. DOI: 10.1016/j.eurpolymj.2008.05.033.
153. Mohr, P. J; Taylor, B.N; and Newel, D.B.(2008). CODATA Recommended Values of the Fundamental Physical Constants, *Reviews of Modern Physics*, 80(2), pp. 633-730.
154. Douglas, B; Mc. Daniel, D; and Alexander, J. (1994). *Concepts and Models of Inorganic Chemistry*, 3rd. Edition, John Wiley & Sons, New York, pp. 771-778.
155. Wongmanerod, C; Zangooie, S; and Arwin, H. (2001). Determination of Pore Size Distribution and Surface Area of Thin Porous Silicon Layers by Spectroscopic Ellipsometry. *Applied Surface Science*, 172, pp. 117-125. PII: S1069-4332(00)00847-3.
156. Ahluwalia, V. K. and Parashar, R. K. (2007). *Organic Reaction Mechanism*, 3rd. Edition, Alpha Science, Oxford, pp. 1-2, 8-10, 16-17, 78-86, 96-98, 233-255.

157. Wibawa, P. J., Agam, M. A. Nur, H. and Saim, H. (2010). Changes in Physical Properties and Molecular Structure of Polystyrene Nanospheres Exposed with Solar Flux. *Enabling Science and Nanotechnology AIP Conference Proceeding*, 1341, pp. 54-61. DOI:10.1109/ESCINANO.2010.5701028.
158. Steiner, Erich (2008). *The Chemistry Maths Book*, 2nd .Edition, Oxford University Press, Oxford, pp.15-43, 80-87, 126-146.
159. Jibril, M; Noraini, J. and Poh, L.S. (2013). Removal of Color from Waste Water Using Coconut Shell Activated Carbon (CSAC) and Commercial Activated Carbon (CAC), *Jurnal Teknologi (Sciences and Engineering),* 60, pp. 15-19.
160. Syafalani S; Abustan, I; Dahlan, I; Wah, C.K. and Umar, G. (2012). Treatment of Dye Wastewater Using Granular Activated Carbon and Zeolit Filter, *Modern Applied Science*, 6(2), pp. 37-51.
161. Chen, Y; Zhou, S. and Li, Q. (2011). Mathematical Modeling of Degradation for Bulk-Erosive Polymers: Application in Tissue Engineering Scaffolds and Drug Delivery Systems, *Acta Biomaterialia*, 7, pp.1140–1149. DOI: 10.1016/j.actbio.2010.09.038.
162. Ma, J; Liu, Y; and He, H. (2010). Degradation Kinetics of Anthracene by Ozone on Mineral Oxides, *Atmospheric Environment*, 44, pp. 4446–4453. DOI: 10.1016/j.atmosenv.2010.07.042.
163. Titus, M. P; Molina, V. G; Baños, M. A; Giménez, J. and Esplugas, S. (2004). Degradation of Chlorophenols by means of Advanced oxidation Processes: a General Review, *Applied Catalysis B: Environmrntal*, 47, pp. 219–256. DOI: 10.1016/j.apcatb.2003.09.010.
164. Kirkan, B. and Gup, R. (2008). Synthesis of New Azo Dyes and Copper (II) Complesxes Derived from Barbituric Acid and 4-Aminobenzoylhydrazone, *Turkey Journal of Chemistry*, 32, 9-17.
165. Tang, H; Wang, S; Pan, M; and Yuan, R. (2007). Porosity-Graded Micro-Porous Layers for Polymer Electrolyte Membrane Fuel Cells. *Journal of Power Sources*, 166, pp. 41-46. DOI: 10.1016/j.jpowsour.2007.01.021.
166. Schooneen M.A.A; Xu, Y; and Strongin, D. R. (1998). An introduction to Geocatalysis, *Journal of Geochemical Exploration*, 62(1-3), pp. 201-215.
167. Wilkinson, F. (1980). *Chemical Kinetics and Reaction Mechanism*, Van Nostrand Reinhold Co. Ltd. New York, pp. 132-135.

168. Wang, Y; Zhuang, C; Wu, C; Zhang, J; Wang, L; Xin, M; Zhu, G. and Xu, J. (2011). The Synthesis, Structure and Photoluminescence Property of a Novel 3D Supramolecular Compound Based on Mixed Ligands of 8-Hydroxyquinoline-5-sulfonate and Ethylenediamine. *Journal of the Serbian Chemical Society*, 76(11), pp. 1497-1504.

169. Glasgovich, N. (2012). *Infrared Spectroscopy: Spectral Analysis-Sulfonate*. URL source : http://www.chemistry.ccsu.edu/glagovich/teaching/316/ir/sulfonate.html. Retrieved: March 18, 2012.

170. Mohammed, I.S. and Mustapha (2010). A. Synthesis of New Azo Compounds Based on N-(4-Hydroxypheneyl) maleimide and N-(4-Methylpheneyl) maleimide, *Molecules*, 15, pp. 7498-7508.